

LASER'S AND OPTICS IN ATMOSPHERIC REMOTE SENSING



09 - 11 September 2015

***Venue: Physics Seminar Room
3rd Floor, H-Block, Westville***

Organized by



UNIVERSITY OF KWAZULU NATAL

SPONSORS



Workshop Programme

09 September 2015

14:00-17:00	Laser Safety Course	Dr. Aletta Karsten
18:00-20:00	Braai (for outside participants)	

Venue : H-Block, Braai area, Westville

10 September 2015

08:00-08:30	Registration	Miss Lulu Raxangana
	Breakfast (for outside participants)	
08:45-09:00	Introduction to the workshop	Prof. Sivakumar Venkataraman
09:00-09:45	Atmospheric Remote Sensing – Basics	Prof. Sivakumar Venkataraman
09:45-10:30	LiDAR for atmospheric observations	Prof. Hassan Bencherif
10:30-11:00	Tea Break	
11:00-11:30	LiDAR as a measurement tool-S.A's first LiDAR system - Dr. Aletta Karsten	
11:30-12:00	CSIR-NLC mobile LIDAR	Mr. Lerato Shikwambana
12:00-12:30	Durban LiDAR	Dr. Nkanyiso Mbatha
12:30-13:00	UKZN-3-D Portable LiDAR	Prof. Sivakumar Venkataraman
13:30-14:00	Lunch Break	
14:00-14:45	CDTA – ALGERIA LIDAR?	Dr. Mohammed Traiche
14:45-15:30	Laser based optical communications in free space	Dr. Yaseera Ismail and Miss. Sharmini Pillay
15:30-15:45	Tea Break	
15:45-16:30	Group-1 : Visit to UKZN LIDAR system	Mr. Jerremiah Ogunniyi & Prof. Siva
15:45-16:30	Group-2 :Visit to Laser based optical communication lab	Dr. Yaseera Ismail and Miss. Sharmini Pillay
16:30-17:15	Group-2 : Visit to UKZN LIDAR system	Mr. Jerremiah Ogunniyi & Prof. Siva

16:30-17:15	Group-1 : Visit to Laser based optical communication lab	Dr. Yaseera Ismail and Miss. Sharmini Pillay
17:30-19:00	Braai – H Block Braai Area	

11 September 2015

08:30-09:00	Breakfast(outside participants)	
09:00-09:45	Atmospheric aerosol retrieval using Sun-Photometer	Dr. Adesina Joseph
09:45-10:30	Solar Radiometry	Miss Paulene Govender
10:30-11:00	Tea Break	
11:00-11:45	Group-1 : Visit to UKZN Sun Photometer system	Dr. Adesina Joseph & Miss Priyanka Singh
11:00-11:45	Group-2 : Visit to Solar Radiometry	Miss Paulene Govender and Mr. Jeremiah Ogunniyi
11:45-12:30	Group-2 : Visit to UKZN Sun Photometer system	Dr. Adesina Joseph & Miss Priyanka Singh
11:45-12:30	Group-1 : Visit to Solar Radiometry	Miss Paulene Govender and Mr. Jeremiah Ogunniyi
12:30-13:30	Lunch Break	
13:30-15:30	Lecture on Light and Light based Technologies Prof. Jon Rash, Prof. Francesco Petruccione, Prof. Thomas Konrad and Others	
15:30-15:45	Tea Break	
	Closure	

UNIVERSITÉ DE LA RÉUNION
Toujours un temps d'avance

METEO FRANCE

CATS

LiDAR for atmospheric observations

Prof. Hassan BENCHERIF

Laboratoire de l'Atmosphère et des Cyclones - LACY
UMR 8105 CNRS / Université de La Réunion / Météo-France

Reunion Island
20.8°S, 55.5°E

ATMRESET 2015, 10-11 September, UKZN, Westville, Durban H. BENCHERIF, Reunion University

outlines

- **Introduction:** fundamentals on Earth's atmosphere
 - Vertical structure and composition
 - Tropospheric and stratospheric circulations
- **LiDAR experiment**
 - Principal and LiDAR equation
 - Measurements: temperature and aerosols profile retrievals
- **Applications**
 - LiDAR experiments at Maïdo observatory, Reunion Island
 - Recent observations:
 - Case study: large-scale volcanic aerosol transport following the Chile's Calbuco eruption on April 2015

ATMRESET 2015, 10-11 September, UKZN, Westville, Durban H. BENCHERIF, Reunion University

introduction



- The atmosphere is the most external gaseous envelope of our planet Earth.
- It is transparent to light radiations in the visible range and protects us (and the biosphere) from incoming solar UV radiations.
- In fact, only part of the solar radiation reaches the Earth's surface and controls all physical and photo-biological processes.
- Similarly, a small part of the emitted IR radiations escapes to space
- The Earth's atmosphere acts then like filter in 2 directions: it filters incoming and outgoing radiations
- The atmosphere is a major component of the climate. It is responsible for the greenhouse effect that warms the Earth.



ATMRESET 2015, 10-11 September, UKZN, Westville, Durban H. BENCHERIF, Reunion University

vertical structure

Earth's atmosphere is about 100 km thick, but most of it is within 16 km from the surface. Air pressure decreases with altitude.

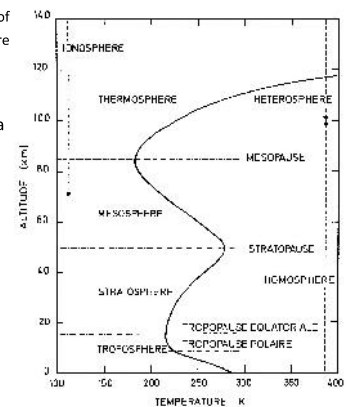
- @ sea level, air pressure is about 1013 hPa
- @ 15 km height, air pressure is about 100 hPa
- @ 30km height, it decreases to about 10 hPa

The Earth's atmosphere is divided into 3 main layers, depending on the temperature gradient:

- the TROPOSPHERE,
- the STRATOSPHERE,
- the MESOSPHERE

separated successively by dynamical barriers

Tropopause, Stratopause and Mesopause



ATMRESET 2015, 10-11 September, UKZN, Westville, Durban H. BENCHERIF, Reunion University

chemical composition

atmospheric gases (dry air)	Volumes (%)	M. molaires (g.mol ⁻¹)
↳ Nitrogen (N ₂)	78,09	28,016
↳ Oxygen (O ₂)	20,95	32,000
↳ Argon (Ar)	0,93	39,944
↳ Carbone dioxide (CO ₂)	0,035	44,010
↳ Neon (Ne)	1,8 10 ⁻³	20,183
↳ Helium (He)	5,24 10 ⁻⁴	4,003
↳ Methane (CH ₄)	1,79 10 ⁻⁴	16,04
↳ Hydrogen (H ₂)	5,0 10 ⁻⁵	2,016
↳ Ozone (O ₃)	1,0 10 ⁻⁶	48,000
↳ Radon (Rn)	6,0 10 ⁻¹⁸	222,00
↳ Water Vapour (H ₂ O)	de 1 % à 4 % (variable)	18,01

> The Earth's atmosphere is a complex mixture of several "gases", either atomic or molecular in nature.

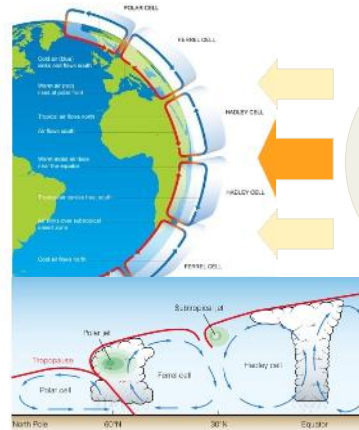
> Air consists primarily of N₂ (78%) and O₂ (21%), with small amounts of several other substances, including Argon (0.9%).

> In most cases, the atmosphere behaves like an ideal gas in hydrostatic equilibrium.

> Constant Components: proportions remain the same over time and location.

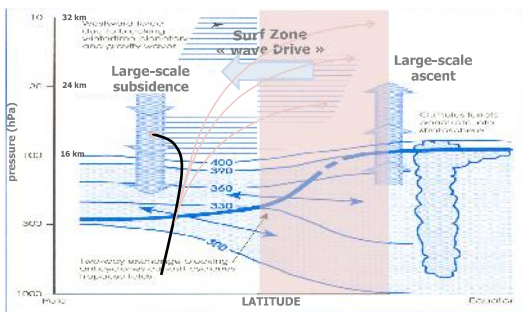
> Variable Components: amounts vary over time and location

tropospheric circulation



- Atmospheric circulation is a large-scale movement of air, and the means by which thermal energy is distributed on the surface of the Earth
- Due to the shape and inclination of the Earth, the solar flux received at the surface is not uniform. It depends (among others) on location (latitude).
- The incoming solar flux is greater in the tropics than in the polar regions
- The Earth rotation (*Coriolis force*) results in an overall air circulation made of three cells: **Hadley, Ferrel and Polar** cells

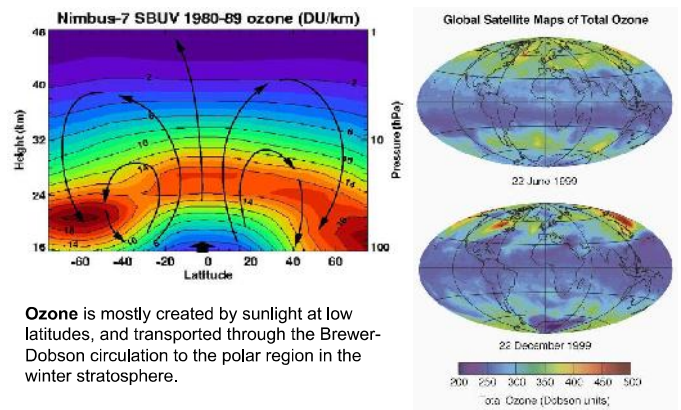
stratospheric circulation



adapted from Holton et al. (1995)

- The BD circulation is a large-scale stratospheric cell. It results from interaction between planetary waves and the mean-zonal flow.
- In the LS, planetary and gravity wave breaking may occur in the form of large-scale exchange events between the STR and mid-latitudes.

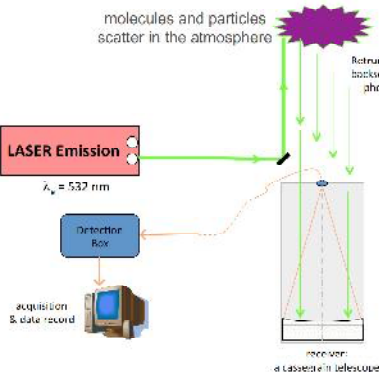
stratospheric circulation



Ozone is mostly created by sunlight at low latitudes, and transported through the Brewer-Dobson circulation to the polar region in the winter stratosphere.

principal of LiDAR

LiDAR is an acronym for **Light Detection And Ranging**



- Light is emitted by a mono- or a poly-chromatic laser beam and scattered and attenuated by molecules, aerosols (dust), and cloud (water or ice) particles in the atmosphere
- A LiDAR system transmits short pulses of laser light into the atmosphere.
- The returned signal is collected by a telescope and directed into a detection box
- The laser and associated detection box specifications depend on the targeted component or parameter.

ATMRESET 2015, , 10-11 September, UKZN, Westville, Durban H. BENCHERIF, Reunion University

principal of LiDAR

LASERS

- Lasers are categorized by their wavelength. 600-1000nm lasers are commonly used for non-scientific purposes but, as they can be focused and easily absorbed by the eye, the maximum power has to be limited to make them 'eye-safe'.
- For atmospheric LiDAR experiments there are different laser sources, depending on the targeted component or parameter
- The laser beam must not be attenuated by the atmosphere. The emitted and received wavelength should lie in a spectral transmission window of the atmosphere
- Most of LiDAR systems use the fundamental wavelength 1064nm produced by Nd:YAG lasers
> the most used derived wavelengths are obtained by doubling or by tripling the fundamental, what produces laser pulses at 532nm (a green beam) and at 355nm (in the UV)

ATMRESET 2015, , 10-11 September, UKZN, Westville, Durban H. BENCHERIF, Reunion University

principal of LiDAR

Example (1)

> Rayleigh LiDAR system

It uses ONE laser source and it is based on interactions between the emitted laser beam and atmospheric components: molecules (Rayleigh) and particles (Mie) back-scatter

- > Time resolution less than 1 ms
- > Vertical resolution less than 100m
- > Repetition rate: variable (10 Hz, 20 Hz, 30 Hz, 50 Hz)
- > Altitude range: from ground to 70-80km



Spectra Physics Quanta Ray LAB 150-10 Nd:YAG

@ 1064 nm	8-12 ns, 650 mJ/pulse
@ 532 nm	1-2 ns, 300 mJ/pulse
@ 355 nm	2-3 ns, 270 mJ/pulse
@ 266 nm	3-4 ns, 180 mJ/pulse

ATMRESET 2015, , 10-11 September, UKZN, Westville, Durban H. BENCHERIF, Reunion University

principal of LiDAR

Example (2)

- DIAL system

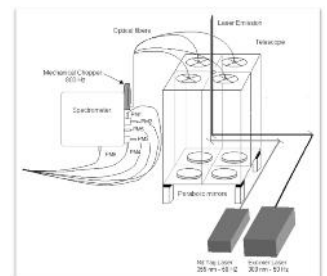
DIAL stands for *Differential Absorption LiDAR*

It uses TWO laser sources and it is also based on interactions between the emitted laser beam and atmospheric components.

A DIAL system requires the use of a pair of emitted wavelengths:

- an absorbed wavelength (λ_{on})
- a non-absorbed wavelength (λ_{off})

- > Time resolution less than 1 μ s
- > Vertical resolution less than 100m
- > Repetition rate: variable
- > Altitude range: 10-45km



For OZONE monitoring by a DIAL system, the 3rd harmonic of a Nd:YAG laser is used to provide the λ_{off} (355nm), and an XeCl Excimer laser could generate the absorbed wavelength λ_{on} (308nm)

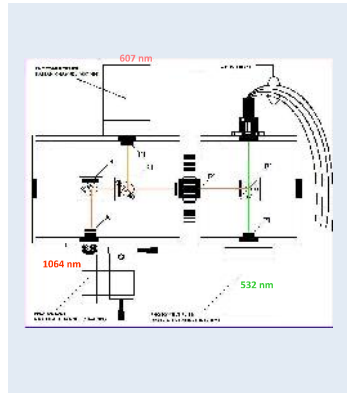
ATMRESET 2015, , 10-11 September, UKZN, Westville, Durban H. BENCHERIF, Reunion University

principal of LiDAR

Example of detection box

a multi-channel LiDAR detection box :

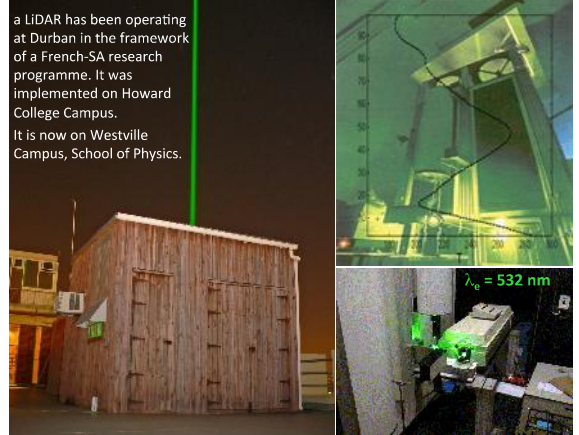
- Rayleigh-Mie at 1064 nm,
- Rayleigh-Mie at 532 nm, and
- Raman-N₂ at 532/607 nm



ATMRESET 2015, , 10-11 September, UKZN, Westville, Durban H. BENCHERIF, Reunion University

LiDAR experiments

a LiDAR has been operating at Durban in the framework of a French-SA research programme. It was implemented on Howard College Campus. It is now on Westville Campus, School of Physics.



ATMRESET 2015, , 10-11 September, UKZN, Westville, Durban H. BENCHERIF, Reunion University

LiDAR equation

The LiDAR signal may result

- ▶ from an elastic return signal with no change in the wavelength: $\lambda_{\text{emission}} = \lambda_{\text{reception}}$
It is the case for Rayleigh-Mie LiDARs (based on the principle of Rayleigh and Mie photon scattering)
- ▶ from an inelastic backscattered signal: $\lambda_{\text{emission}} \neq \lambda_{\text{reception}}$
This is the case for Raman-N₂ LiDARs (based on the Raman shift due to molecular nitrogen vibrations)

The backscattered signal equation has the following expression:

$$S(z) = K \frac{\beta_r(z, \lambda_e)}{(z - z_0)^2} \cdot T^2(z, \lambda) \cdot \Delta z$$

Atmosphere density

- β is the backscatter coefficient : $\beta(z, \lambda) = \mathbf{n}(z) \cdot \sigma(\lambda)$ (σ is the backscatter cross-section)
- T^2 is the atmos. transmission coefficient : $T^2(z, z_0) = \exp\left[-\int_{z_0}^z [\alpha(u, \lambda_e) + \alpha(u, \lambda_r)] du\right]$
- α is the extinction coefficient, it depends on the emission and return wavelengths

ATMRESET 2015, , 10-11 September, UKZN, Westville, Durban H. BENCHERIF, Reunion University

LiDAR equation and retrieval

$$S(z) = K \cdot \frac{T^2(z, z_0)}{(z - z_0)^2} \cdot n(z) \cdot \sigma \cdot \Delta z$$



$$n(z) = K \cdot S(z) \cdot (z - z_0)^2 \cdot T^2(z, z_0)$$

$T^2(z, z_0)$ is the atmospheric transmission coefficient between z and the top of the atmosphere z_0 .

Temperature and aerosol profiles can then be derived from the LiDAR back-scattered signal by initializing the pressure parameter at the top of the profile with an external value (a climatological model, for example).

ATMRESET 2015, , 10-11 September, UKZN, Westville, Durban H. BENCHERIF, Reunion University

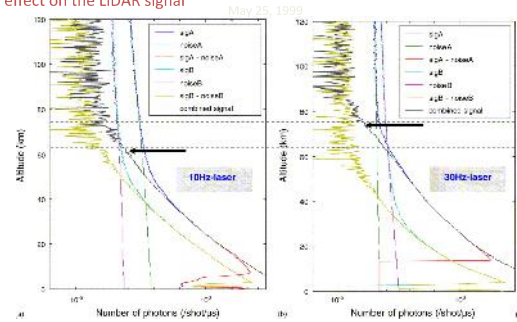
LiDAR equation and retrieval

Some important corrections ...

- Aerosols' and ozone attenuation
- PM saturation: non-linearity of the counting mode
- Pressure initialisation at the top of the profile
- Signal merging, if any
- Parametrization of the back-ground noise
- Time-integration and statistical error
- ...

LiDAR equation and retrieval

Sampling effect on the LiDAR signal

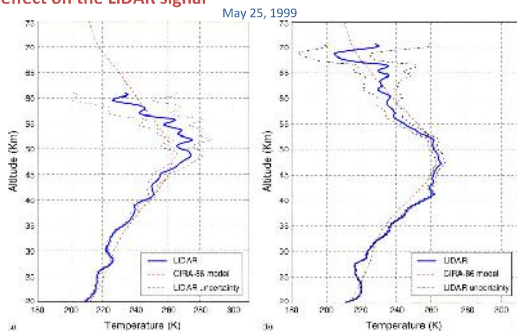


Comparison of channel A (sigA) and channel B (sigB) return signals obtained with a 10- and 30-Hz lasers, respectively. Both lasers were run for the same period, i.e., 5.5 hours. The first profile (left) is averaged over 198,000 laser shots of the 10Hz laser, while the second profile (right) is averaged over 594,000 laser shots of the 30Hz laser.

Moorgawa et al. (2007), UKZN PhD

LiDAR equation and retrieval

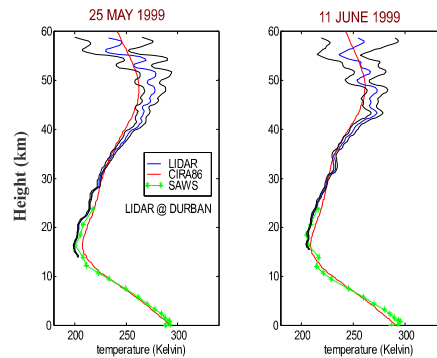
Sampling effect on the LiDAR signal



Comparison of the LiDAR and climatological model (CIRA-86) temperature profiles for 25 May 1999 obtained with (a) 10Hz laser and (b) 30Hz laser. Both profiles are obtained after five and a half hours of LiDAR acquisition.

Moorgawa et al. (2007), UKZN PhD

LiDAR equation and retrievals

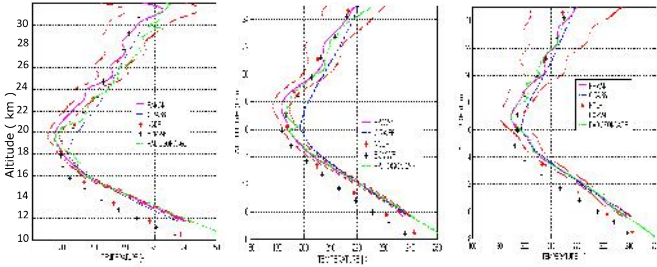


Comparison of LiDAR and SAWS temperature profiles obtained over Durban on 25 May and 11 June 1999. The corresponding CIRA-86 monthly climatological profiles are superposed.

Tropopause and stratopause heights are obtained at **16.5 km** and **48 km**, respectively.

The wave-like structures appearing above 40 km result from gravity and planetary waves propagation.

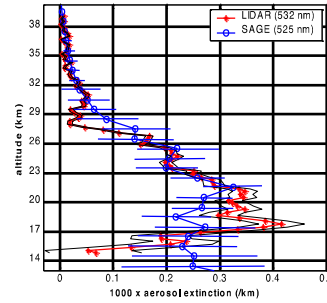
LiDAR equation and retrievals



Comparison of temperature profiles obtained by Raman-N₂ LiDAR and quasi-simultaneous and co-localised radiosonde measurements.

Bencherif et al. (2010)

LiDAR equation and retrievals



LiDAR and SAGE II aerosol extinction profiles recorded quasi-simultaneously, on June 8, 1999 (at 532 nm and 525 nm, respectively). The horizontal lines represent SAGE II error bars, while the LiDAR profile is framed by the aerosol extinction profiles at $\pm\sigma$, total uncertainty.

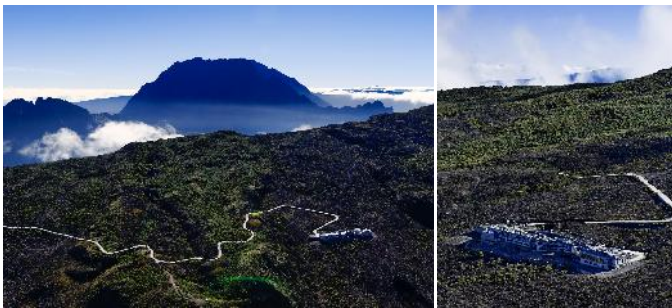
Bencherif et al. (2003)

Validation of a Rayleigh-Mie LiDAR at Durban (30°S, 30°E), South Africa

→ In addition to LiDAR validation, the study evidences a stratospheric layer made of back-ground aerosols. The observed aerosol layer extends up to ~30km and indeed overlaps with the stratospheric ozone layer.

Maïdo Observatory

The Maïdo Observatory is a research facility dedicated to atmospheric observations. It is located on the west side of Reunion Island at 2200 m asl. All of the instruments implemented at Maïdo are of international standard and are operational in framework of international observational networks such as **NDACC** (Network for the Detection of Atmospheric Composition Changes) **SHADOZ** (Southern Hemisphere Additional OZonesondes).



Maïdo Observatory

Mean objectives

- ❖ Permanent station for long-term atmospheric observations:
 - to study dynamic and chemistry of the troposphere and the stratosphere in the context of climate change in the SH.
 - > Temperature, ozone, UV Radiations, H₂O, GHG, aerosols, ... continuous monitoring
- ❖ Provide data for international research - monitoring networks
- ❖ Provide data for national and international scientific research programmes in collaboration with partners such as SA scientists in the framework of the GDRI ARSAIO
- ❖ Provide data for satellite calibration and validation: OMI, AURA, ENVISAT, METOP (IASI, GOME2), MEGHATROPIQUES, ADM-AEOLUS, ...

Education / Summer School

Due to its geographic position in the southern tropics and taking into account its high level of equipment for atmospheric observations and science, Reunion Island is a well adapted training platform to welcome scientists and young scientists from African and the Indian Ocean countries.

The first Maïdo Summer School is planned to take place on **November 2016** and intended to focus on observation/instrument training together with selected lecturing on processes and changes in the Earth's atmosphere (troposphere and stratosphere) with emphasis on dynamics, long-term evolution of atmospheric composition and climate change.



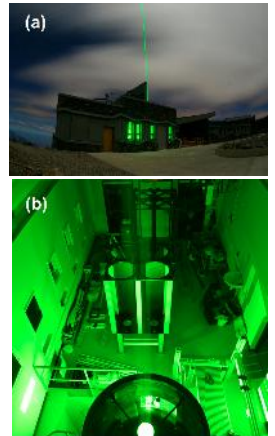
ATMRESET 2015, , 10-11 September, UKZN, Westville, Durban H. BENCHERIF, Reunion University

There are two multi-channels LiDAR systems operating at the Maïdo Observatory:

- A Rayleigh-Mie-Raman LiDAR system to measure aerosol, temperature, water vapour and tropospheric ozone profiles
- a DIAL system to monitor stratospheric ozone profiles

(a) Outside-view on the station during LiDAR operation

(b) Inside-view on LiDARs room at Maïdo



ATMRESET 2015, , 10-11 September, UKZN, Westville, Durban H. BENCHERIF, Reunion University

RMR LiDAR (RMR: Rayleigh - Mie - Raman)

It is the largest/highest LiDAR system designed to monitor water vapour up to the Lower Stratosphere. The Reunion RMR LiDAR is an innovative system designed to measure the atmospheric H₂O, which is a very important component but difficult to monitor in the Earth's atmosphere due to its inhomogeneous vertical distribution. > 99% of atmospheric water vapour is found in the troposphere.

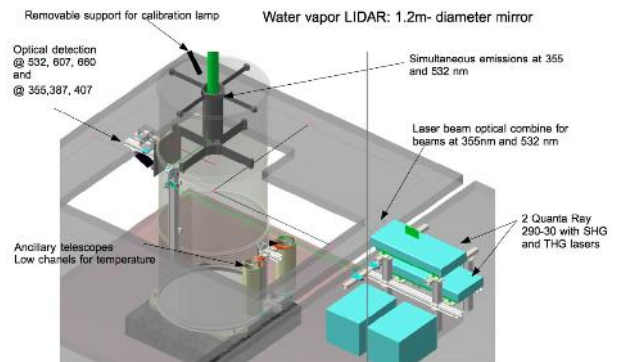
The RMR LiDAR is designed to stand TWO wavelength (355nm and 532nm) and TWO lasers.



ATMRESET 2015, , 10-11 September, UKZN, Westville, Durban H. BENCHERIF, Reunion University

RMR LiDAR (RMR: Rayleigh - Mie - Raman)

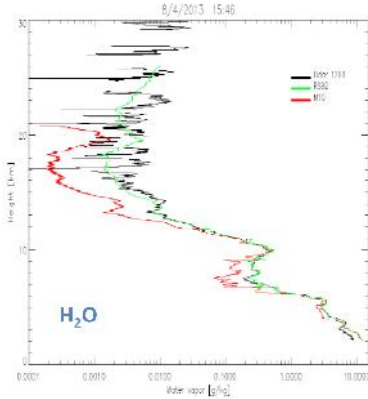
a multi-channel and multi-parameter system ...



ATMRESET 2015, , 10-11 September, UKZN, Westville, Durban H. BENCHERIF, Reunion University

LiDAR experiment at Maïdo Observatory

RMR LiDAR (RMR: Rayleigh - Mie - Raman)



Quasi-simultaneous profiles of **water vapour** mixing ratio obtained with RMR LiDAR and radio-sonde experiments at Maïdo Observatory, Reunion Island, on 8 April 2013

ATMRESET 2015, 10-11 September, UKZN, Westville, Durban H. BENCHERIF, Reunion University

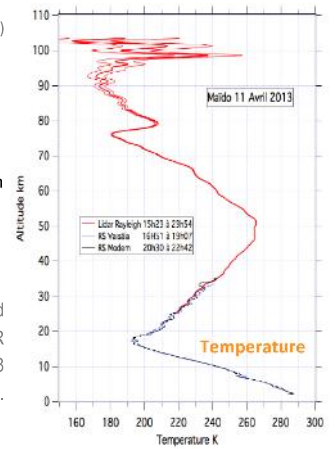
LiDAR experiment at Maïdo Observatory

RMR LiDAR (RMR: Rayleigh - Mie - Raman)

The RMR Lidar has been operating at Maïdo since **October 2012**

- Radiosondes (Modem M10) are weekly performed from Reunion Airport (8 m asl)
- Vaisala RS92 and Modem M10 have been launched from the Maïdo site on April 2013 during the MALICCA campaign (Maïdo LiDAR Calibration Campaign)

Quasi-simultaneous and co-localized temperature profiles obtained with RMR LiDAR and radiosondes at Maïdo on 11 April 2013 during the MALICCA campaign.



ATMRESET 2015, 10-11 September, UKZN, Westville, Durban H. BENCHERIF, Reunion University

Application: Recent LiDAR Observations

a case study:

large-scale volcanic aerosol transport following the Chile's Calbuco eruption on April 2015


by the use of ground-based and satellite observations over southern Africa and Indian Ocean




to be developed during the workshop ...

ATMRESET 2015, 10-11 September, UKZN, Westville, Durban H. BENCHERIF, Reunion University

ATMRESET 2015, 10-11 September, UKZN, Westville, Durban H. BENCHERIF, Reunion University




UNIVERSITY OF KWAZULU NATAL



Atmospheric Remote Sensing – Basics


Prof. Venkataraman. Sivakumar
Discipline of Physics

School of Chemistry and Physics
 Discipline of Physics
 Email : venkataramans@ukzn.ac.za
 Web : physicsdbn.ukzn.ac.za/Research/Atmosphere.aspx
atmres.ukzn.ac.za/home.html



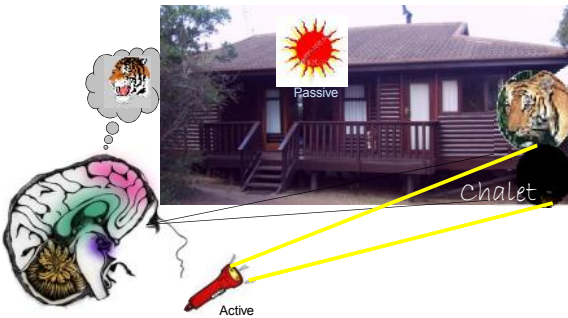
AtmRes @ UKZN <http://atmres.ukzn.ac.za/home.html> Siva

Remote ????



The Eye as a Remote Sensing Instrument

- Eyes are scanning the environment with up to 60 frames per second



Chalet

Active

Passive

What is Remote Sensing ?

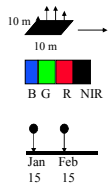
Remote Sensing is the **SCIENCE** and **ART** of obtaining **INFORMATION** about an **OBJECT**, **AREA**, or **PHENOMENON** a device that is **NOT IN CONTACT** with through the analysis of **DATA** acquired by the object, area, or phenomenon under investigation.

AtmRes @ UKZN

<http://atmres.ukzn.ac.za/home.html>

Siva

Remote Sensor Resolution



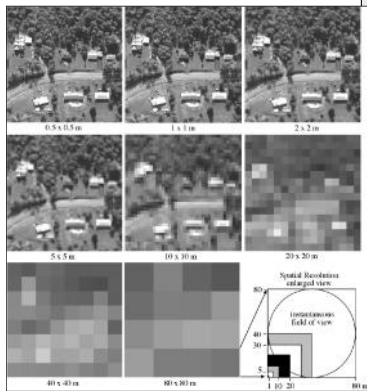
- Spatial - the size of the field-of-view, e.g. 10 x 10 m.
- Spectral - the number and size of spectral regions the sensor records data in, e.g. blue, green, red, near-infrared, thermal infrared, microwave (radar).
- Temporal - how often the sensor acquires data, e.g. every 30 days.
- Radiometric - the sensitivity of detectors to detect small differences in electromagnetic energy.

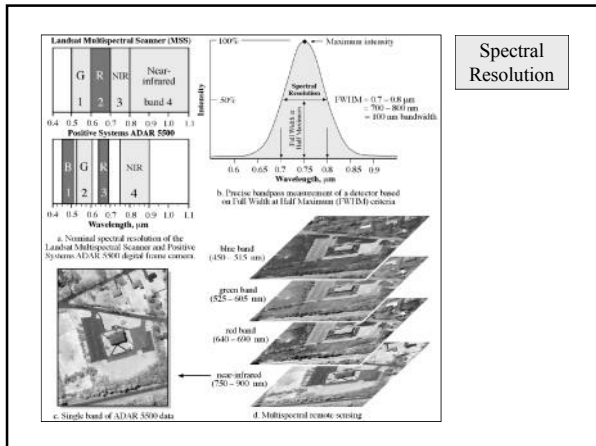
AtmRes @ UKZN

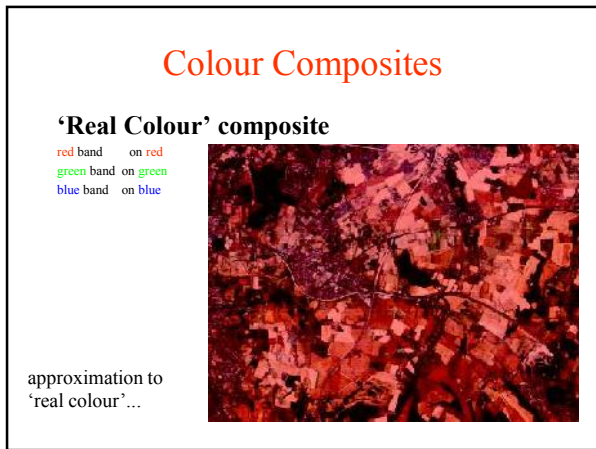
<http://atmres.ukzn.ac.za/home.html>

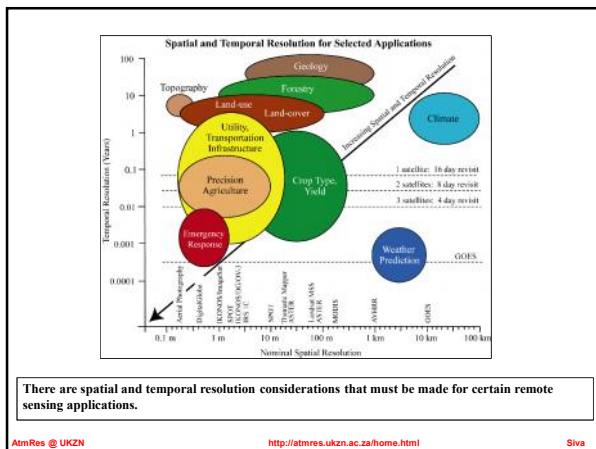
Siva

Spatial Resolution







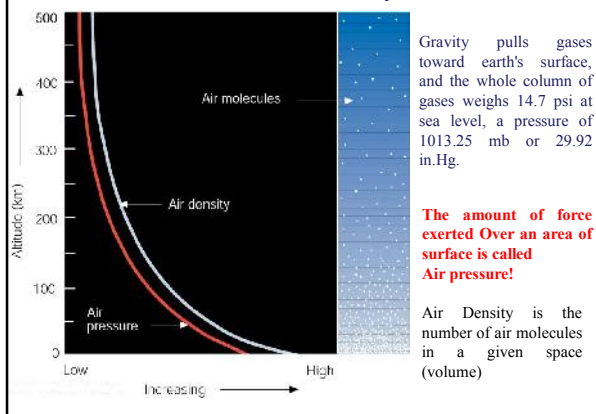


There are spatial and temporal resolution considerations that must be made for certain remote sensing applications.

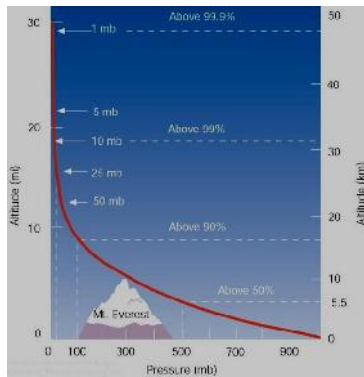
Composition of Atmosphere

- Nitrogen - 78%
- Oxygen - 21%
- Water Vapor - 0 to 4%
- Carbon Dioxide - .037%
- Other gases make up the rest

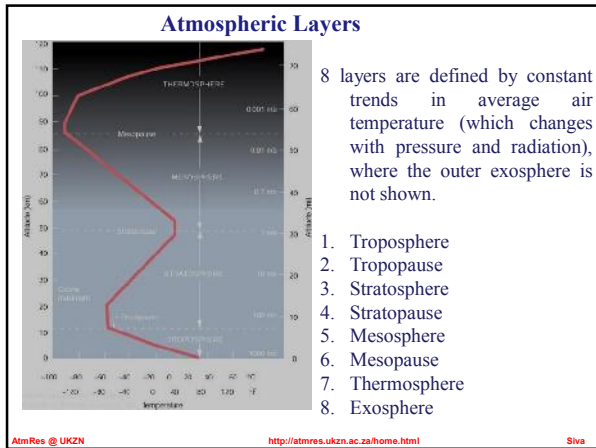
Pressure & Density

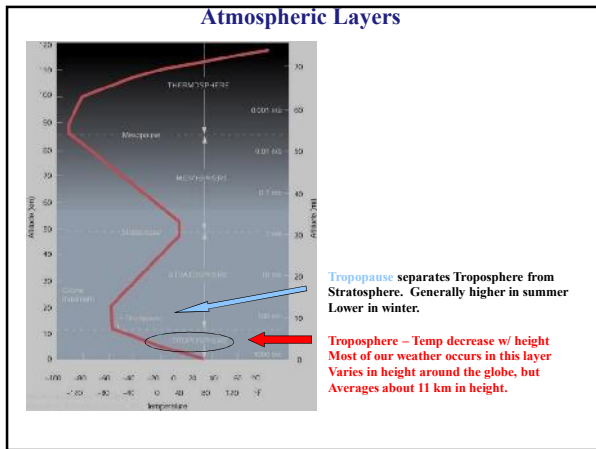


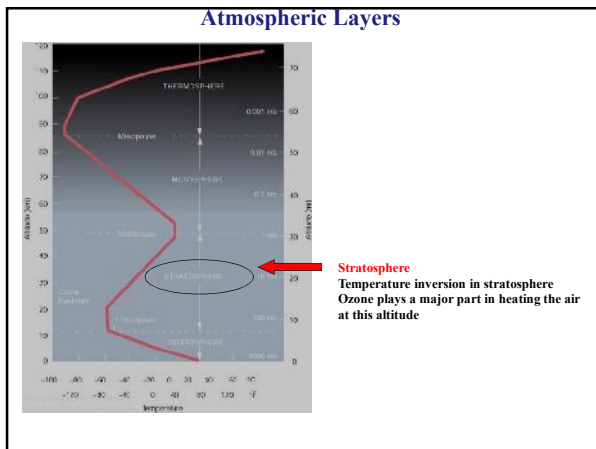
Vertical Pressure Profile



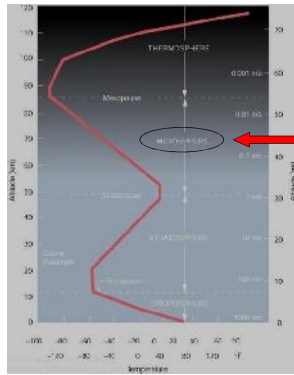
Atmospheric pressure decreases rapidly with height.







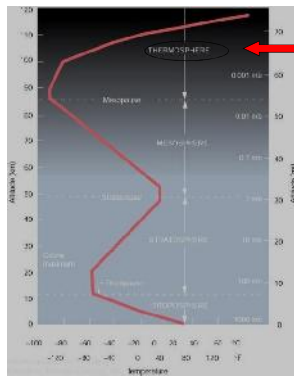
Atmospheric Layers



Mesosphere

Middle atmosphere – Air thin, pressure low, Need oxygen to live in this region. Air quite Cold -90°C (-130°F) near the top of mesosphere

Atmospheric Layers



Thermosphere

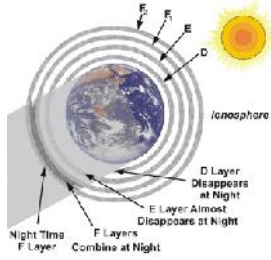
“Hot layer” – oxygen molecules absorb energy from solar Rays warming the air. Very few atoms and molecules in this Region.

The Ionosphere

- Region of charged ions (positive) and electrons
- Electrons are torn off atoms by sunlight of short wavelengths
- Electrons don't recombine easily because the distance between molecules is large at high altitudes and collisions are not frequent

Layers of the Ionosphere

- Lowest part: D layer has enough collisions to cause it to disappear after sunset.
- Remaining ions and electrons recombine, without sunlight new ones are no longer produced.
- Layer return at sunrise



Weather & Climate

Weather is comprised of the elements of:

- a) air temperature
- b) air pressure
- c) humidity
- d) clouds
- e) precipitation
- f) visibility
- g) wind

Climate represents long-term (e.g. 30 yr) averages of weather.

LIDAR as a measurement tool – South Africa's first LIDAR system

Aletta Karsten
National Measurement Institute of South Africa (NMISA)

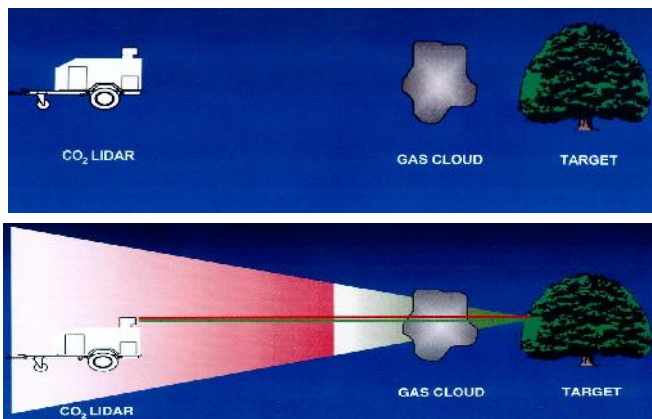
Your measure of excellence

Content

- DIAL principle
- Description of the first DIAL system manufactured in SA
- Improvements
- Detection in forests

© NMISA 2014

The DIAL principle



© NMISA 2014

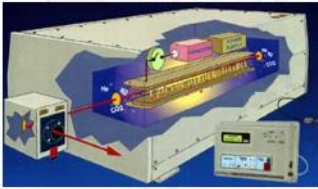
Advantages of remote detection

- Non-interfering
- Integrated-path measurements
- Measurements at ground level or any altitude above ground
- Measurement over large geographical areas
- Can be done “covertly”

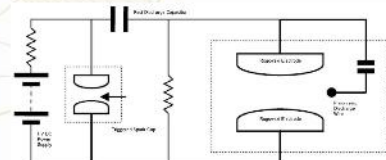
© NMISA 2014

Brief history

- Started 1989
- First benchtop technology demonstrator in 1991. Used as proof of concept
- Developed mini CO₂ TEA laser
 - Transversely exited atmospheric laser
 - Developed electrode profiles, manufacture tube from machineable ceramics



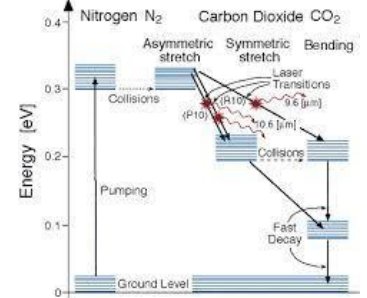
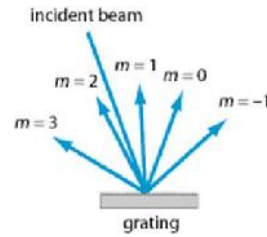
© NMISA 2014



nmisa
National Metrology Institute of South Africa

Tunable CO₂ TEA laser

- > 75 distinct different wavelengths from 9.2 to 10.8 μm by using a diffraction grating



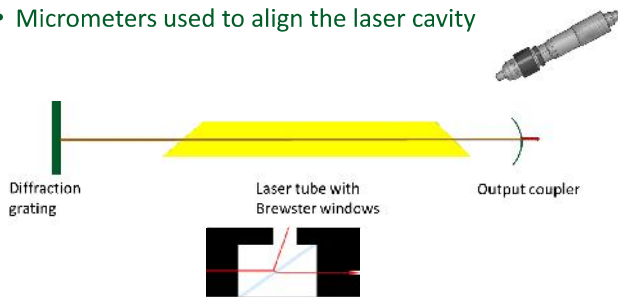
- 17th order of HeNe laser nearly co-inside with 10.6 μm

© NMISA 2014

nmisa
National Metrology Institute of South Africa

Laser layout

- Laser layout (ZnSe Brewster windows to seal off the gas and grating for tunability)
 - Micrometers used to align the laser cavity

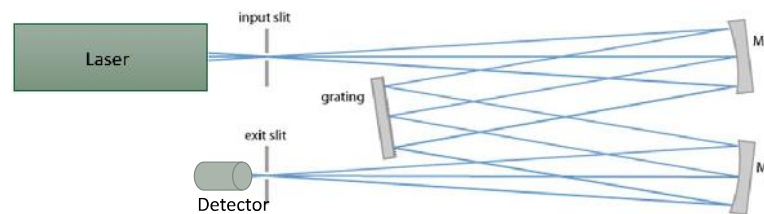


- Gas mixture: CO₂ and He

© NMISA 2014

nmisa
National Metrology Institute of South Africa

Wavelength measurement



© NMISA 2014

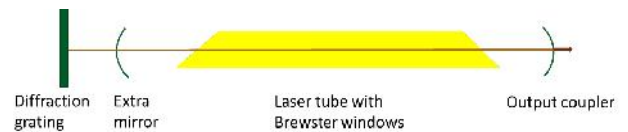
nmisa
National Metrology Institute of South Africa

Detectors

- No commercial detectors available that were sensitive enough to detect the back scattered light
- Cryocooled HgCdTe
 - Locally manufacture and cooled with liquid nitrogen (32 pin connectors)
 - Need to build into a Faraday cage to reduce electronic noise
 - Improve SNR

Improvements on the system

- From 1994 onwards expand wavelength range with the addition of $^{13}\text{CO}_2$
 - Increase wavelength range, could now measure between 9.2 and 11.3 μm
 - Addition of middle mirror



- Build system into horsebox trailer
- Test integrated path measurements as method to detect gasses form industrial areas – perimeter detection



© NMISA 2014



© NMISA 2014

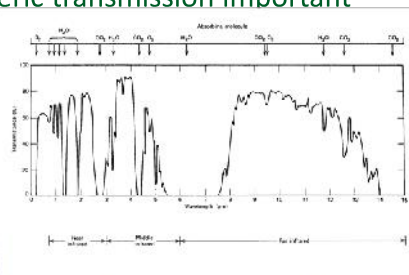


Expansion of the system

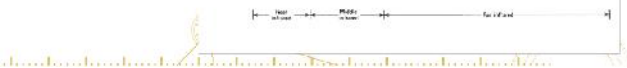
- BVOC – measurements – highly volatile
 - Measurements in a tube
 - Wind a problem
 - Plastic covers (Glad Wrap)
 - Damp generator
 - Irrigation pipes along the length of the pipe/tunnel
 - Large metrological balloon filled with gas and then released
- The 4 laser bands available on the present system:
- Band 1: CO_2 Laser: wavelengths between 9.2-10.8 micron
- Band 2: Alexandrite resonator is tunable between 720 and 800 nm.
- Band 3: Second harmonic of Alexandrite laser provides tunability between 360 and 400 nm and
- Band 4: the third harmonic of the Alexandrite laser provides tunability from 240 to 266 nm

Limitations of the system

- Takes time to tune the laser wavelengths between the 4 different laser bands as well as within Bands 3 and 4. Inside Band 1 and Band 2 the tuning is fast. We are investigating automating tuning within band 3 and 4.
- Atmospheric transmission important

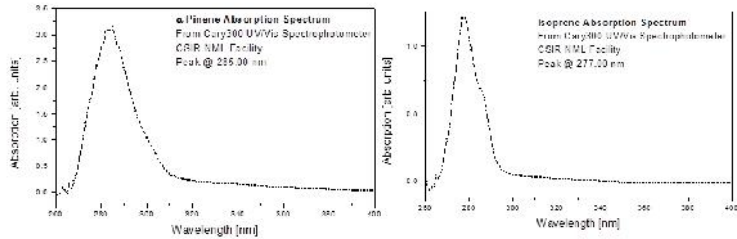


© NMISA 2014



Species of interest

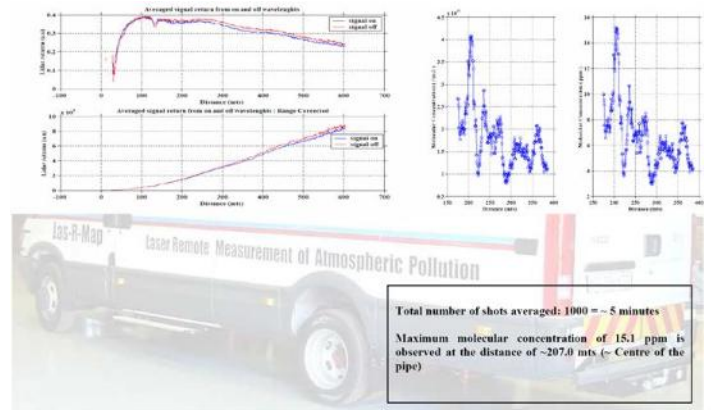
- Request from forestry to measure Isoprenes and Pinenes to determine forest growth remotely



© NMISA 2014



SO₂ measurements



© NMISA 2014



The mobile system



Methods to contain gas during measurements



© NMISA 2014



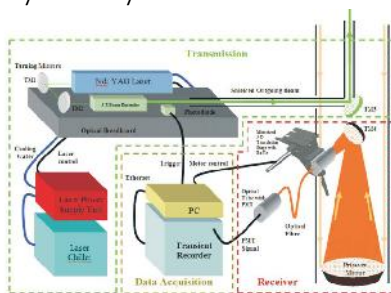
CSIR-NLC MOBILE LIDAR SYSTEM



HISTORY

- In 2003 the CSIR developed a Differential Absorption LIDAR (DIAL) for the purpose of measuring particular gases in the atmosphere, such as carbon dioxide and sulphur dioxide.
- In mid - 2000 the CSIR LIDAR system was altered with a focus to study the lower atmosphere.
- In early 2007 the operations of the new layout of the system began.
- The main aim of the system was to study aerosols, clouds, water vapour and temperatures for heights less than 30km.

System layout



Specifications of the LIDAR system

PARAMETER	DESCRIPTION
Transmission	ALFA ROMEO
Laser source	532 nm
Operating wavelength	700 nm (at 500 m/s)
Beam diameter	0.1 m
Pulse width	7 ns
Pulse repetition rate	10 Hz
SCAN CHARACTERISTICS	1/2 ROTATION PER SECOND
MEASUREMENT	Measurement
Resolution	0.1 m
Scan rate	0.5 m/s
Field of view	360 degrees (horizontal) / 120 degrees (vertical)
Range	0.2 km
Signal and data processing	Signal
Receiver	APD
Detector	APD
Non-destructive	0.1 m
Powerful computer	Intel Core i7-4770K @ 3.4 GHz
Operating system	Windows 7
Software platform	Matlab

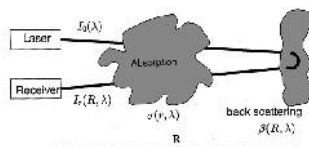


Shock-absorber frame and Hydraulic feet



- The air-filled bellows mounted to the van floor to provide vibration damping to the aluminium structure.
- Hydraulic stabiliser feet have been added to the vehicle suspension to ensure stability during the measurements. When stationary, the four stabiliser feet can be extended downward, allowing the van to be completely supported and eliminating movements due to the tyres or suspension.

Principles of LIDAR



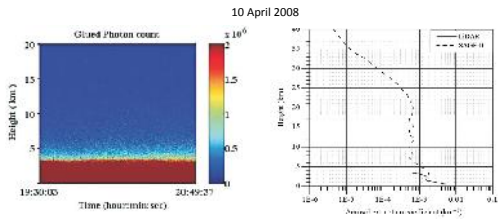
Lidar equation:

$$I_r(R, \lambda) = I_0 \frac{A}{4\pi R^2} \beta(r, \lambda) \exp(-2 \int_0^R \alpha(r, \lambda) dr)$$

β → reflectance or backscattering coefficient (Rayleigh, Mie, Raman fluorescence)

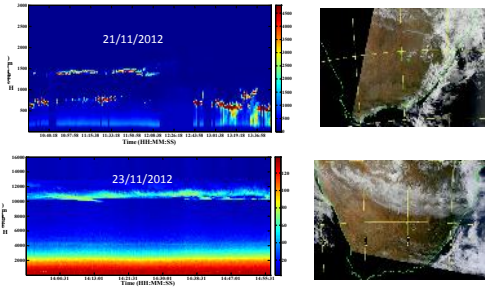
α → extinction coefficient (absorption, scattering)

Some results from the CSIR-LIDAR system: For aerosol studies

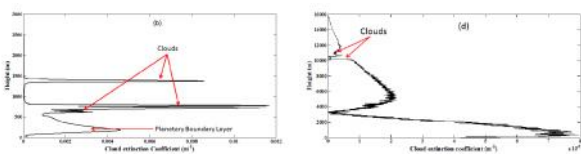


Sivakumar et al 2009: CSIR South Africa mobile LIDAR—First scientific results: comparison with satellite, sun photometer and model simulations, *South African Journal of Science*, 105, 449-455

Some results from the CSIR-LIDAR system: For cloud studies



Some results from the CSIR-LIDAR system: For cloud studies



Date	LIDAR COD
21 November 2012	0.3195
23 November 2012	0.0256

Cirrus clouds are classified into sub-visual (COD < 0.03), optically thin (COD between 0.03 and 0.3), and thick (COD > 0.3)

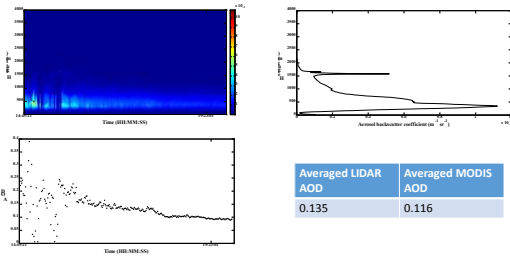
The beginning of the upgrade process



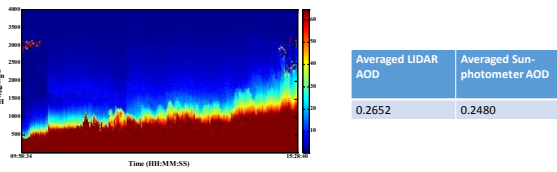


Some results from CSIR-LIDAR system with the scanner: For aerosol studies

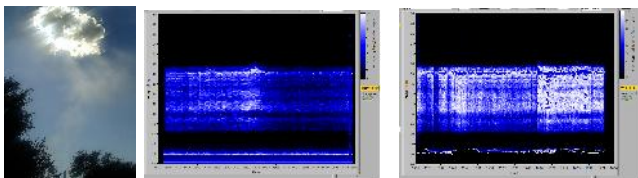
11 February 2013, Stellenbosch

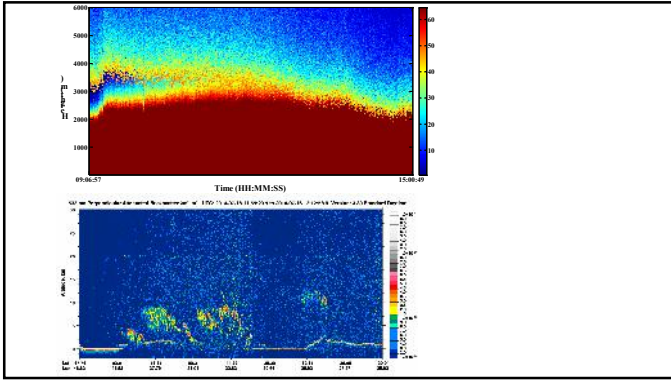


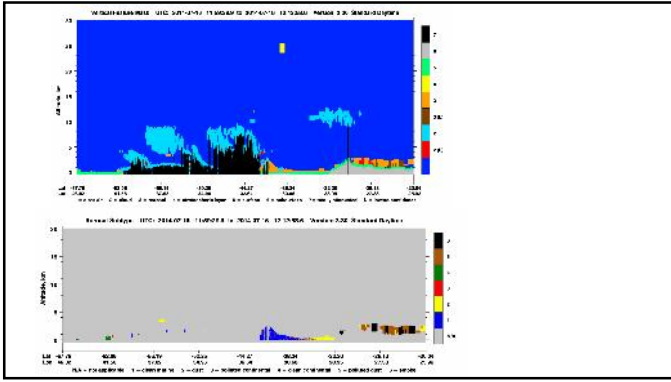
27 June 2014, Pretoria



15 May 2014, Lephalale







Thank You!

The Durban LIDAR: Atmospheric Remote Sensing

Nkanyiso Mbatha² and Venkataraman Sivakumar¹

¹School of Physics, University of KwaZulu-Natal, Durban 4000, South Africa
²South African Weather Service (SAWS), PO Box 320, Stellenbosch, 7599



Outlines

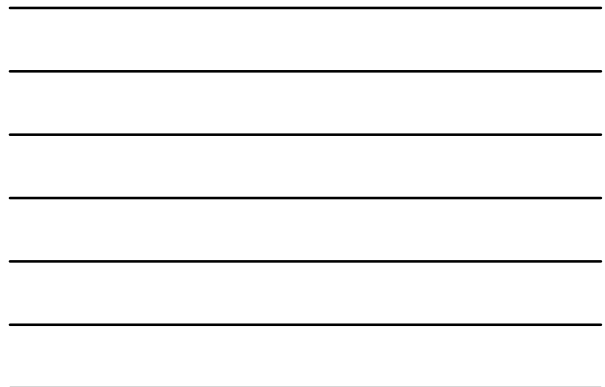
- Introduction
- Basic Principle of operation
- The actual instrument
- Data and results

Type of LIDAR: Target Quantity

- **Applications:**
- altimeter
- Rayleigh Lidar: temperature
- DIAL (Differential Absorption)-Lidar: trace gases
- multi wavelength aerosol Lidar: aerosol amount and aerosol properties (size distribution, type)
- Raman-Lidar: trace gases
- Doppler-Lidar: particle velocities
- Fluorescence-Lidar: temperature in the upper atmosphere

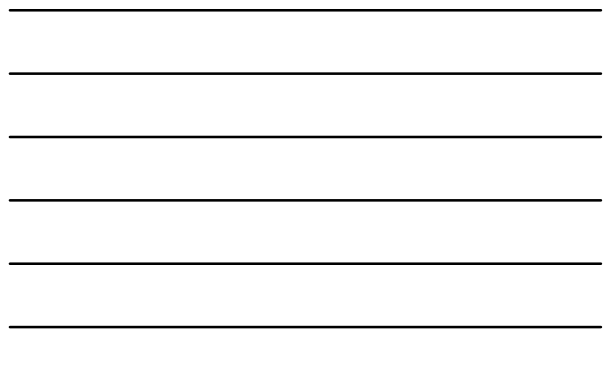
The Durban LIDAR

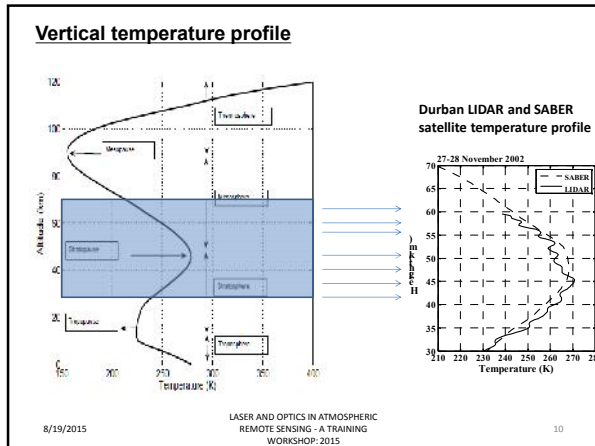
- First installation in April 1999 (Nd:YAG laser at a repetition rate of 10 Hz).
- In May 2002, the 10 Hz laser was replaced with a more powerful Nd:YAG delivering at least 5 times more power and operating at a frequency of 30 Hz. Table 1 compares the characteristics of the two lasers.
- The system was implemented on the campus of the University of Nata within the framework of a bi-lateral Franco-South African cooperation (Service d'Aeronomie of CNRS, Laboratoire de Physique de l'Atmosphère of Reunion Island University and UKZN).
- The system is a Rayleigh-Mie type.

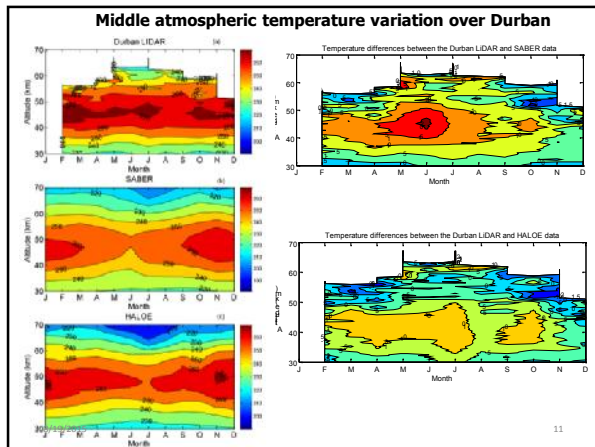


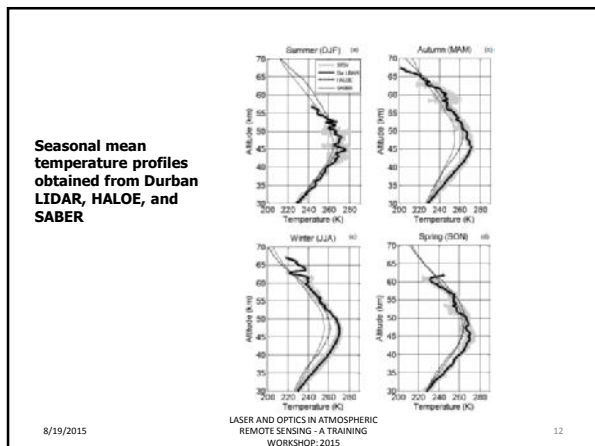
Parameters	
Excimer laser	10-100 Hz
Excimer laser pulse width	10-15 ns
Excimer laser pulse energy	200 mJ
Excimer laser pulse diameter	120 mm
Excimer laser pulse duration	1-2 ns

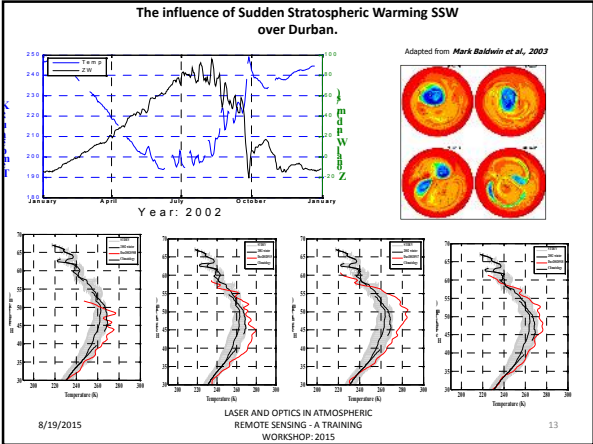
Plot of the Durban LIDAR raw data for 21 May 2002 where the electronic shutters were set at 60 μs. The total noise (green line) is parameterised as a parabolic curve over the altitude range 100–150 km. The useful signal (red line) is that from which the total noise is subtracted.

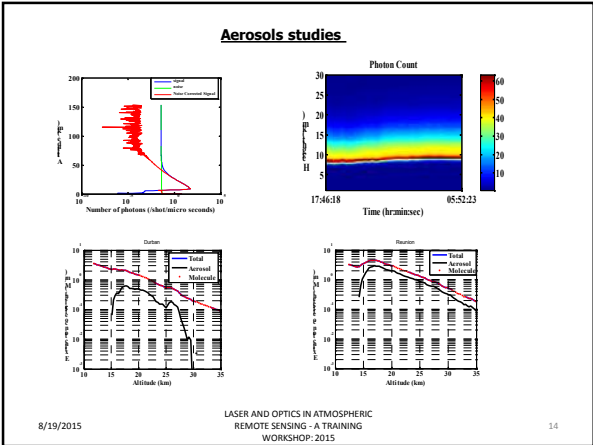














Future Work

- Continuous middle atmospheric temperature measurements
- Improve the LIDAR
- LIDAR Gravity waves studies

8/19/2015 LASER AND OPTICS IN ATMOSPHERIC REMOTE SENSING - A TRAINING WORKSHOP: 2015 15





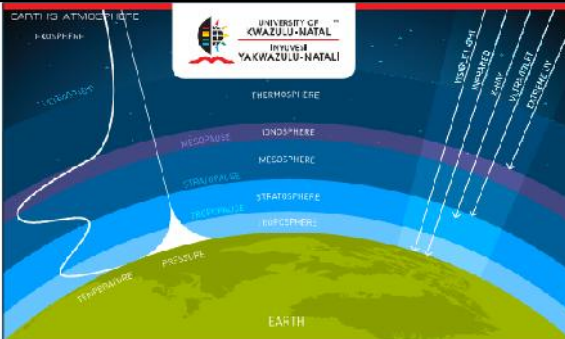
UNIVERSITY OF KWAZULU NATAL

A new 2-D portable Durban LiDAR for atmospheric studies

Prof. Venkataraman, Sivakumar
Discipline of Physics

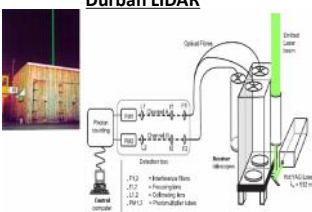
School of Chemistry and Physics
Discipline of Physics
 Email : venkataramans@ukzn.ac.za
 Web : physicsdbn.ukzn.ac.za/Research/Atmosphere.aspx
 atmres.ukzn.ac.za/home.html



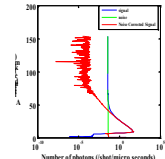


ATMOSPHERIC RESEARCH (ATM-RES)
 @ University of KwaZulu-Natal, School of Chemistry and Physics

Durban LIDAR

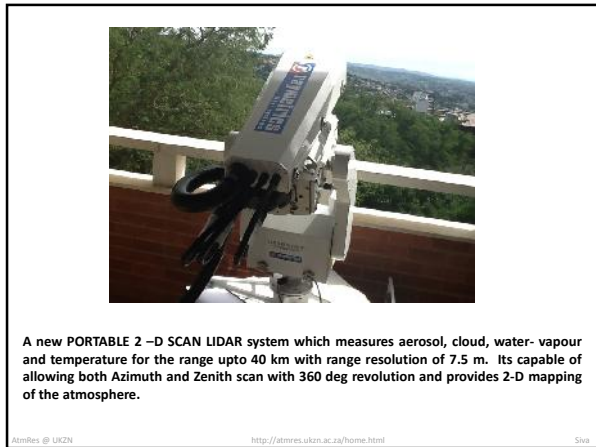


Parameter	Value
Wavelength	1064 nm
Pulse duration	10 ns
Repetition rate	100 Hz
Beam diameter	10 cm
Receiver diameter	10 cm
Receiver FOV	100 mrad
Receiver NA	0.01
Receiver area	0.00785 m²
Receiver efficiency	0.1
Receiver gain	1000
Receiver noise	1000
Receiver bandwidth	100 MHz
Receiver dynamic range	100 dB
Receiver range	100 km
Receiver resolution	10 m
Receiver accuracy	10 m
Receiver stability	10 m
Receiver reliability	100%
Receiver cost	100,000 R



Plot of the Durban LIDAR raw data for 21 May 2002 where the electronic shutters were set at 60 μ s. The total noise (green line) is calculated over the altitude range 100–150 km. The useful signal (red line) is that from which the total noise is subtracted.



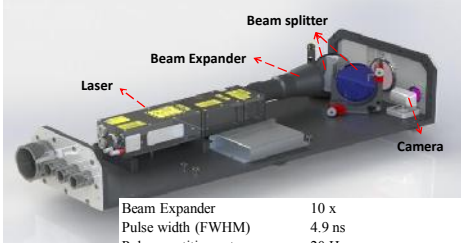


Parameters	Specifications
Transmitter	
Laser Source	Nd:YAG - Quantel®
Operating Wavelength	355 nm
Average pulse energy	35 mJ (at 355 nm)
Beam Diameter	3.4 mm
Beam Expander	10 x
Pulse width (FWHM)	4.9 ns
Pulse repetition rate	20 Hz
Beam Divergence	0.97 mrad before Beam Expander 0.097 mrad after Beam Expander
Q-Switch Delay	145 µs
Receiver	
Telescope type	Cassegrain
Diameter	200 mm (Primary), 48 mm (Secondary)
Focal Length	800 mm
Field of View	0.5 mrad
PMT	Hamamatsu® R7400-U20
Optical fibre	Multimode, 600 µm core
Filter FWHM	0.7 nm
Signal and Data Processing	
Model	Lice® TR20
Memory Depth	16384
Maximum Range	122.880 km
Spatial Resolution	7.5 m
PC	
TR15-40 Interface	Ethernet
Processor	Intel® Core2Duo 2.6 GHz
Operating system	Windows® XP Pro
Software Interface	NI LabVIEW®

Portable UKZN Durban LIDAR

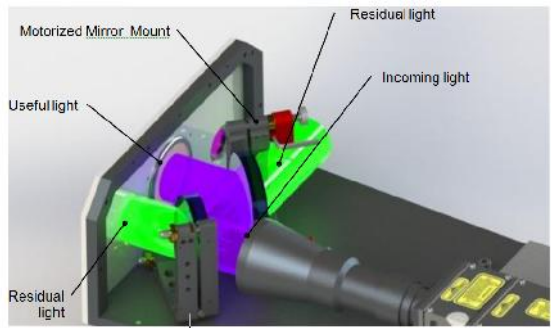
LASER : QUANTEL ULTRA 100 SERIES

Laser Source Nd:YAG - Quantel®
Operating Wavelength 355 nm
Average pulse energy 35 mJ (at 355 nm)
Beam Diameter 3.4 mm



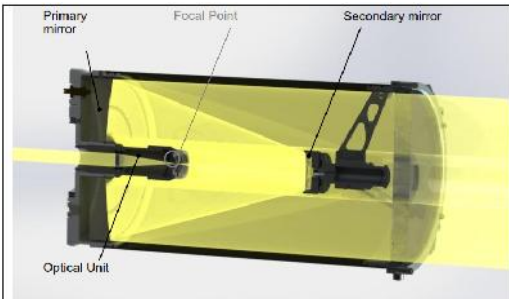
Beam Expander 10 x
Pulse width (FWHM) 4.9 ns
Pulse repetition rate 20 Hz
Beam Divergence 0.97 mrad before Beam Expander
0.097 mrad after Beam Expander

LASER : QUANTEL ULTRA 100 SERIES



Receiver

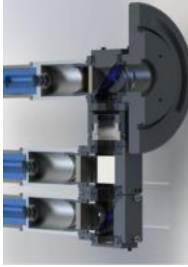
Telescope type Cassegrain
Diameter 200 mm (Primary), 48 mm (Secondary)
Focal Length 800 mm
Field of View 0.5 mrad



Wavelength separation unit

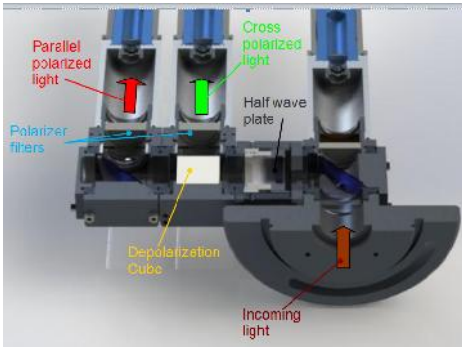


355S 355P 387nm



- PMT** : Hamamatsu® R7400-U20
- Optical fibre** : Multimode, 600 µm core
- Filter** : FWHM 0.7 nm

Wavelength separation unit



Data Acquisition unit



Transient Recorder

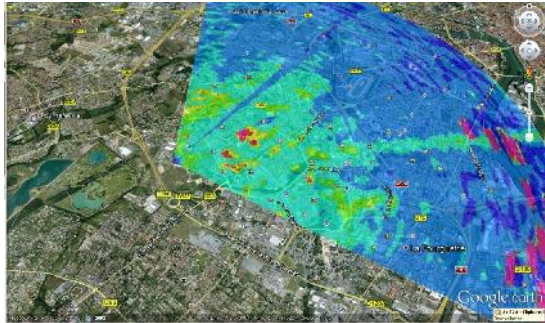


2 AP 2-Axis Sun Tracker / Positioner



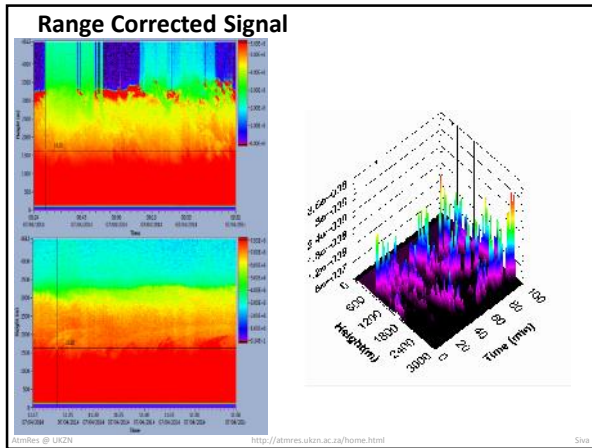
Resolution 0.0025°
Angular Velocity up to 1.8°/sec
Angular Acceleration up to 3.6°/sec²
Torque 40 Nm

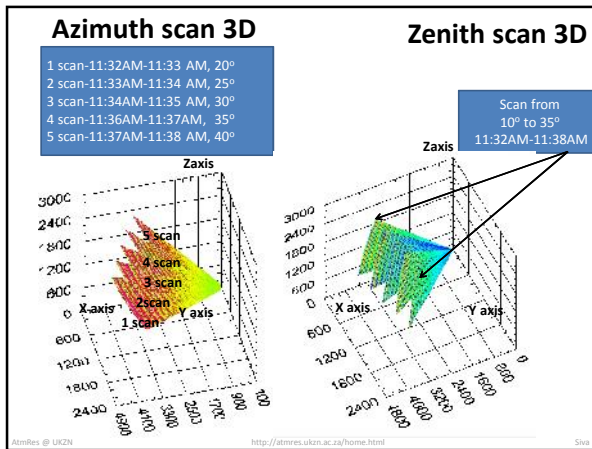
Results on Google Map

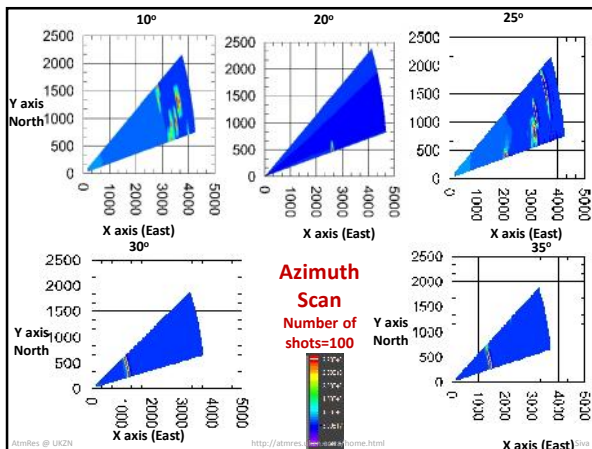


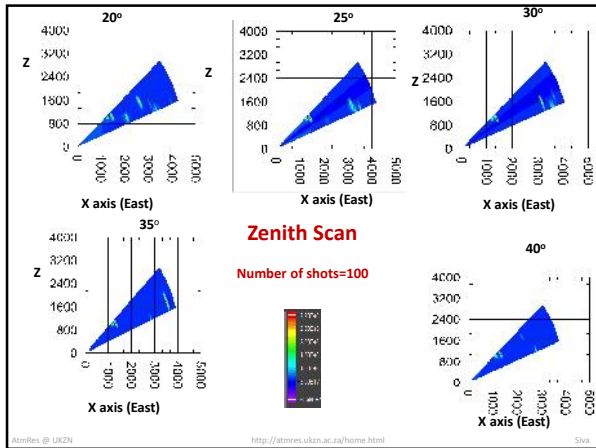
Electrical Cabinet











"After climbing a great hill, one only finds that there are many more hills to climb"
-Nelson Mandela

ATMOSPHERIC RESEARCH (ATM-RES)
University of KwaZulu-Natal, School of Chemistry and Physics

Post Doctoral position is available for LIDAR or LASER and OPTICS specialist !!!

Contact
Prof. Venkataraman. Sivakumar
 School of Chemistry and Physics
 Discipline of Physics
 Email : venkataramans@uzkn.ac.za
 Web : atmres.ukzn.ac.za/home.html

AtmRes @ UKZN http://atmres.ukzn.ac.za/home.html

The LiDAR Based on a Single Optical Pulse Detection

Dr. Mohammed TRAÏCHE

A. Kedadra, R. Guehaz, R. Boudaoud, N. Dermech, H. Lahmar, F. Bouachri

Centre de Développement des Technologies Avancées, Algiers, Algeria
mtraiche@cdta.dz

ATMRES, UKZN, Durban, 10 Sep. 2015

1

Schedule

- I. Introduction : Brief Overview on the Laser Applications
- II. Why the LiDAR is interesting ?
- III. The first application of LiDAR (1962)
- IV. The CDTA LiDAR
- V. The optical pulse as a probe of a physical medium
- VI. The saturation issue
- Conclusion

ATMRES, UKZN, Durban, 10 Sep. 2015

2

I. Introduction : Brief Overview on the Laser Applications

ATMRES, UKZN, Durban, 10 Sep. 2015

3

The laser is applied so as its beam is a carrier of

1. Energy,
2. Heat
3. Information

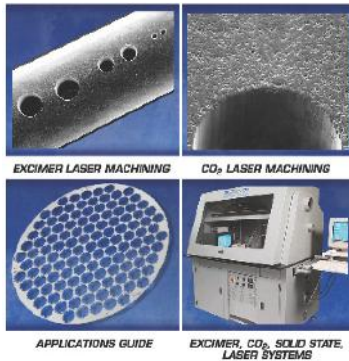
The laser beam carrier of energy to a material

LASER MICROMACHINING GROUP
LASER SYSTEMS GROUP

www.rocontek.com



Photos from the site of



EXCIMER LASER MACHINING

CO₂ LASER MACHINING

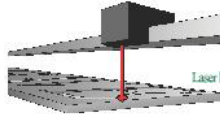
APPLICATIONS GUIDE

EXCIMER, CO₂, SOLID STATE, LASER SYSTEMS

In this case pulsed lasers, UV & fs are utilised

The laser beam carrier of Heat to a Material

Laser engraving



Universal Laser Systems, Inc.

Laser Engraving Manual

Laser cutting



www.laser-cutting-online.com

In Medicine



Esita Ltd.

In this case, cw, IR lasers are utilised ($P \approx$ Watts to tens of kW)

The laser beam carrier of Information to distant material species

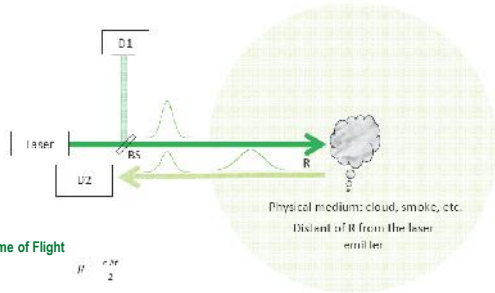
Four techniques are in use

1. Time of Flight detection
2. Phase difference measurement detection
3. Triangulation detection
4. Absolute interferometry detection

7

ATMRES, UKZN, Durban, 10 Sep. 2015

Time of Flight Detection

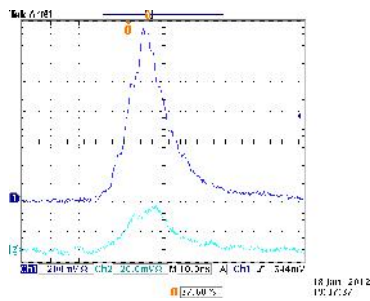


Short pulses (qcq ns) \equiv time of flight \equiv localization of objects and physical phenomena

8

ATMRES, UKZN, Durban, 10 Sep. 2015

The pulse length often is nanosecond ns



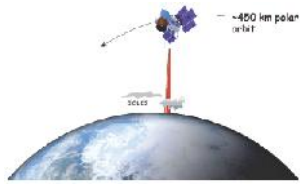
9

ATMRES, UKZN, Durban, 10 Sep. 2015

As a major application: Remote Sensing



R. Schoemaker & K. Benoist: "Characterization of small targets in a maritime environment by means of laser range profiling," SPIE Proc. 8037, 8037051-12, Laser Radar Technology and Applications XVI (2011)



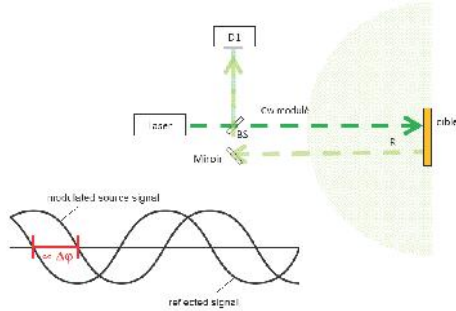
A. W. Yu, M. A. Krainak et al. "Spaceflight laser development for future remote sensing applications," Proc. of SPIE 882, 882041-10, Lidar Technologies, Techniques, and Measurements for Atmospheric Remote Sensing VII (2011)

10

ATMRES, UKZN, Durban, 10 Sep. 2015

Phase difference measurement detection

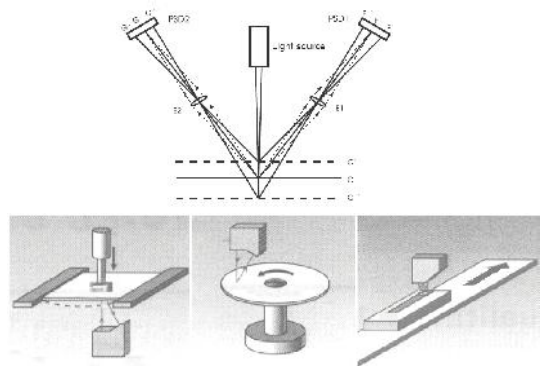
Modulated cw laser distant of a few tens of meters from the target



11

ATMRES, UKZN, Durban, 10 Sep. 2015

Detection by triangulation

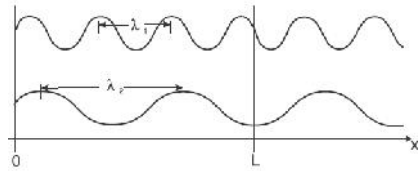


<http://www.lasertechnologies.de>

12

ATMRES, UKZN, Durban, 10 Sep. 2015

Detection by Absolute Interferometry



$$L = \Delta\Phi \cdot \lambda_1 / 2 \quad \frac{\lambda_1 \cdot \lambda_2}{|\lambda_1 - \lambda_2|}$$

13

Comparison

Technique	Time of Flight	Triangulation	Interferometry
Measurement range	10 m to 10s of km	5-200 mm	1 m
accuracy	< 1 mm	0.01 % of measurement range	1 μ m
Emitter	Pulsed laser diode (850-1650 nm)	Collimated laser diode (VIS or NIR) or LED	Tunable laser diode
Detector	Si or InGaAs PIN-photodiode Si or InGaAs APD for longer ranges	PSD CCD array Diode array	Photodiode

From: <http://www.lasercomponents.de>

14

The laser beam carrier of Information on a distant object is applied to:

1. Detection of Echoes from the Moon (Smullin et Fiocco, 1962)
2. The study of Atmosphere (Fiocco 1963, Northend 1966, Clemesha 1967, Sivakumar, 2004, Bhavani Kumar 2010)
3. Meteorological observations (Northend 1966)
4. Study of the Clouds (Grund & Banta 2001)
5. Airborne measurements on wind (Korb 1991, Targ 1996)
6. Analysis of smokes emanating from plant chimeneys (Hamilton 1969)
7. Remote sensing of fire smokes in urban sites (Fennelly 1994)
8. Remote sensing of forest fires smoke (Andreucci 1993, Utkin 2001, Bellecci 2005)
9. Remote sensing of pollutant gases (Edner 1984)
10. Measurements related to climate change (Menzi 1991)
11. Preventing natural hazards: foodings, land slide, earth quacke , and shore corrosion (Ackermann 1999, Guzzetti 2000, Ardizzone 2007).
12. Airborne surveillance of vegetation cover (Tan 2004, He 2011)

15

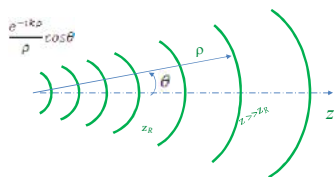
- 13. Time of flight analysis for 3D imaging applied to urban sites (Zhou 2011), open sites (Albota 2002, Oh 2010), and industrial sites (Höfler 1994)
- 14. Quantification of land corrosion and of water level in dums (Fais 2005)
- 15. Classification of land and vegetation (Ding 2011)
- 16. Geologic diagraphy (Yang 2011)
- 17. Management of fishing marine zones (Churnside 2011)
- 18. Extended monitoring of the earth atmosphere (Yu 2011, Komar 2011, Stephan 2011)
- 19. Supervision of space craft autonomous landing (Reiley 1991)
- 20. Etc.

16

II. Why LiDAR is interesting ?

17

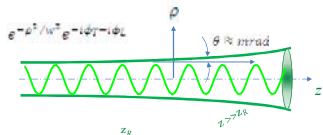
The wave emitted by the RaDAR



✓ Noticeable Divergence along propagation: a few degrees

18

The laser beam



- ✓ Very limited divergence (paraxial propagation)
- ✓ Monochromatic,
- ✓ Temporally coherent (longitudinally),
- ✓ Spatially coherent (transversally).

The laser (light) effect on matter

The light physical effect on matter is exerted through its intensity I expressed in W/cm^2

- So it depends on the intensity transmission.
- In case of a Conventional source:

P is the emitted power. $I = P/4\pi z^2$

- For a Laser beam:

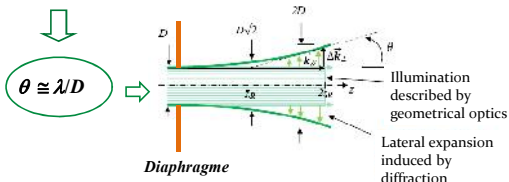
$$I = P/\Omega z^2 = P/\pi\theta^2 z^2$$

With the same power P , the laser exerts an effect

times more important $\xrightarrow{\text{important}}$ Remote Sensing (LiDAR) of the atmosphere



The beam divergence θ



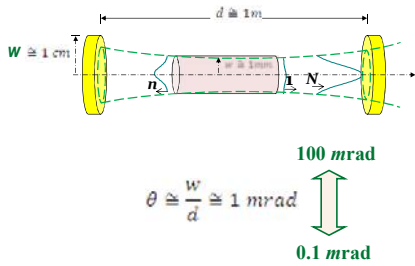
Laser

$\lambda \approx 1 \mu m$
 $D \approx 1 mm - 1 cm$ $\Rightarrow \theta \approx 0.1 \text{ à } 1 \text{ mrad}$

RaDAR

$\lambda \approx 1 \text{ à } 100 cm$
 $D \approx 10 cm \text{ à } 1000 cm$ $\Rightarrow \theta \approx 100 \text{ mrad}$

The divergence θ of a laser beam



In terms of transmitted intensity to farthest distances:

The RaDAR with a spherical wave:

$$\theta_{RaDAR} \approx 1 \text{ deg} \approx 20\,000 \mu\text{rad}$$

The LiDAR with a laser beam :

$$\theta_{Laser} \approx 7'' \approx 40 \mu\text{rad}$$

The LiDAR is more efficient by

$$\left(\frac{\theta_{RaDAR}}{\theta_{Laser}}\right)^2 \approx 10^5 \text{ à } 10^6$$

times.

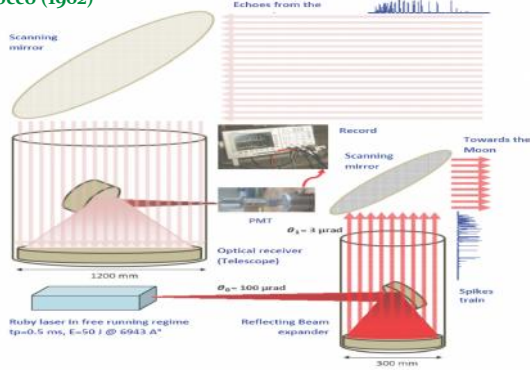
This important aspect among others (interaction with the intra-structure of atoms and molecules) has motivated the use of LiDAR

III. The First Application of LiDAR (1962)

The first LiDAR configuration was performed by Louis D Smullin and Giorgio Fiocco (MIT) and applied to obtain echoes from the Moon (published in Nature 194, 1267, June 30 1962).

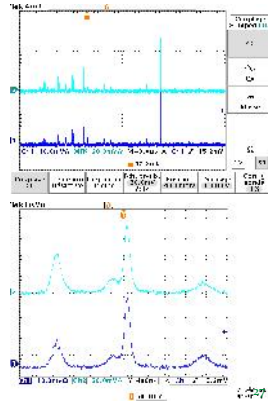
25

The LiDAR configuration as described by Smullin & Fiocco (1962)



26

Ruby laser at CDTA operated in free running regime



Operating parameters compared between Smullin & Fiocco LiDAR and CDTA LiDAR

Operating parameters	CDTA (under development)	LiDAR of Smullin & Fiocco
Laser	Ruby (@6843 nm)	Ruby (@6843 nm)
Laser Energy (J)	1	50
Pulse length (ns)	300	500
Beam expansion	X 1.5*	x10 ** (1000 mm)
Beam Divergence (mrad)	0.3 **	0.3 **
Divergence of the transmitted beam (mrad)	100 *	8 **
Beam width onto Moon land (m)	40	1.2
Laser irradiance onto Moon land (W/cm ²)	~ 0.0	800
Fluence of the laser on telescope PM (J/m ²)	0.3	1.2
The return irradiance at the entrance of the detector (PM II) (W/cm ²)	~ 10 ⁻¹²	30 000 W/cm ² **
Detector (PMT) Photoamplification	Hamamatsu R928 G=10 ⁷	500 G=10 ¹¹ **
Nombre d'électrons à la sortie du détecteur	~ 10 ¹⁴ /tr/10 ¹¹ **	~ 3.1x10 ¹⁰ /tr**
Observation	impossible detection (0 électrons à l'anode)	3% 120 e/40 ns @ PMT anode : one recovered dot $\frac{3}{100} \times \frac{10^7}{10} \times 0.3$

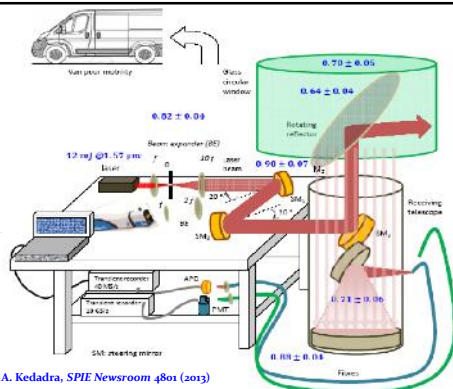
* measured value on CDTA LiDAR

** deduced value from Smullin et Fiocco description.

ATMRES, UKZN, Durban, 10 Sep. 2015

IV- The CDTA Mobile LiDAR

ATMRES, UKZN, Durban, 10 Sep. 2015



M. Traïche, A. Kedra, *SPIE Newsroom* 4801 (2013)

The scheme of the CDTA Mobile LiDAR for Forest Fire Detection CDTA

ATMRES, UKZN, Durban, 10 Sep. 2015

Receiver Telescope Mounting: Newtonian configuration.

Design

Scheme





Development

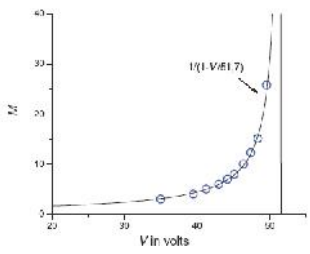



ATMRES, UKZN, Durban, 10 Sep. 2015 34

The detector for the forest fire application
The APD Perkin Elmer C30659-R2H


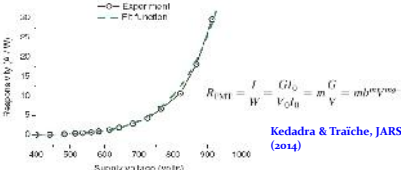


Current gain M vs bias voltage



ATMRES, UKZN, Durban, 10 Sep. 2015 35

The detector for the atmosphere analysis
Hamamatsu (R 928) PMT

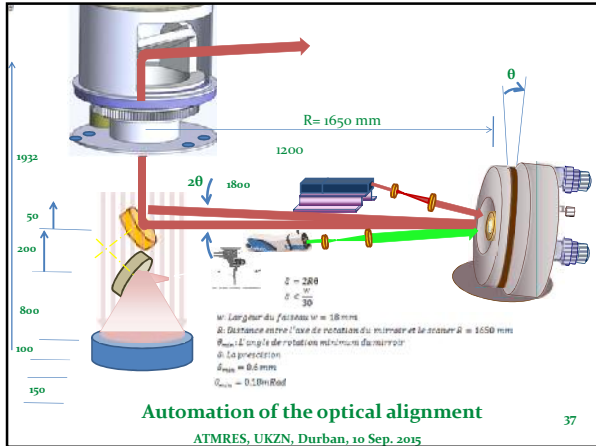



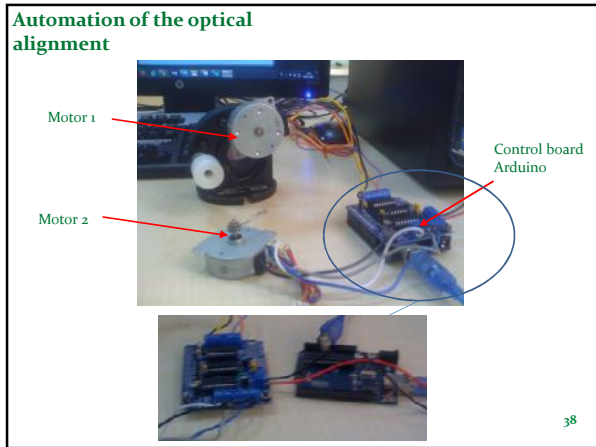
$R_{(341)} = \frac{I}{P} = \frac{G \phi_0}{V_0 \phi_0} = \frac{G}{V_0} = \frac{G}{Y} = \frac{m b^2 V^{2m-1}}{Y}$

Kedra & Traiche, JARS (2014)

Fig. 2 Responsivity plot of the Hamamatsu R928 photomultiplier (PMT) obtained experimentally with a ruby laser at 6943 Å. The fitting function according to Eq. (23) agrees very well with the experimental values with: $m = 0$, $b = 0.31\%$, and $a = 0.978$.

ATMRES, UKZN, Durban, 10 Sep. 2015 36





The CDTA LiDAR instruments and characteristics

Transmitter	LiDAR for forest fire detection	LiDAR for Atmospheric studies
Laser Source	Blue Sky CFB ULE:RA (Nd:YAG / QPO)	Quanta BGM:YAG (SLG)
Operating Wavelength	1,064 nm (avg. 50%)	1064 nm
Energy per pulse (mJ)	10 mJ	1 pulse 400 mJ
Beam width at the laser (mm)	2	5
Beam Expansion	x 10	x 5/8
Pulse length (ns)	7 ns	6 ns
Pulse repetition rate	20 Hz	10 Hz
Beam divergence (mrad)	1	0.3
Refractive index efficiency	0.7	0.5
SP Receiver: Newtonian Telescope		
Focal length (m)	1	
Diameter (cm)	330	
Field of view (degrees)	3	
IF Filter (Bandwidth mm)	0.11	2
The reception efficiency η_r		0.7
Detection & Data Processing		
Detector	APD Photon Counter CCM600 BRAB	PMT Hamamatsu R928
Transmit channel	Fast Counter F408B	Linux TRATHAP
Range Resolution	Resolution 1.5 m	1.5 cm
Atmospheric approximate parameters		
extinction coefficient σ (m ²)		2.5×10^{-4}
The backscattering coefficient β (m ² kg ⁻¹)		2.2×10^{-4}
Data		
Fire smoke	X	X
Temperature	X	X
Water vapor	X	X

ATMRES, UKZN, Durban, 10 Sep. 2015

39

V- The optical pulse as a probe of a physical medium

40

ATMRES, UKZN, Durban, 10 Sep. 2015

The Signal to Noise Ratio (SNR) is the detection criterion

Exact formula

$$\text{SNR}_c = \frac{P_s \text{ Signal power}}{\sqrt{P_q(P_s + P_b + P_n)} \text{ Noise power}}$$

quantum bgnd
internal noise

Si

$$P_s \ll P_b \text{ and } P_n$$

et

$$P_q \approx P_b \mid P_n$$

$$P_q = \frac{hc}{\lambda \sigma \tau_p} = \frac{e}{\tau_p} N_{ph} \quad i_{ph} = \frac{e}{\tau_p} N_{ph}$$

$$P_n = \frac{hc}{\lambda \sigma \tau_p} (i_d + i_{1N} + i_{2N}) \quad I_N = \frac{E_N}{\tau_p}$$

Approximation

$$\text{SNR}_c = \frac{P_s}{P_b \mid P_n}$$

Kedadra & Traïche, JARS (2014)

41

ATMRES, UKZN, Durban, 10 Sep. 2015

Detection by signal addition allows SNR improvement

$$\text{SNR}_c = \frac{P_s}{\sqrt{P_q(P_s + P_b + P_n)}}$$

If

$$P_b = 0, P_n = 0$$

Case of PMT

I returns

$$\text{SNR}_c \approx \sqrt{IP_s}$$

Literature & Kedadra & Traïche, JARS (2014)

42

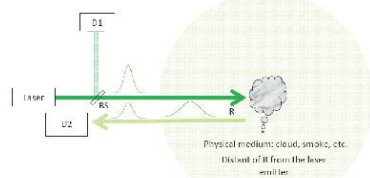
ATMRES, UKZN, Durban, 10 Sep. 2015

However,

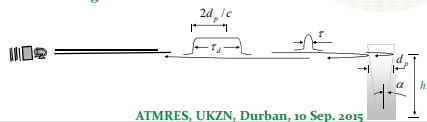
the one ns pulse-based detection allows access to more physical information and ensures automated detection in a least of time.

The return pulse can carry the following information:

1. Localization of the physical object (detection)
2. Determination of the object nature (solid, gaseous, dust, smoke, etc.)
3. The overall size of the physical object (by the scanning capability)
4. Classify the object properties (humid smoke, dry, tree leaves, dust, pure gaz, etc.)



Pulse broadening.



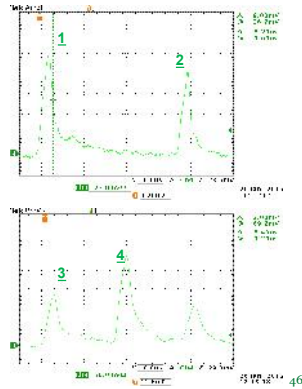
Experiments on fire smoke detection (Nov. 2014-Feb.2015).

Experiments at CDTA on smoke detection by laser and feature extraction in a closed space (with obstacles). November 2014- February 2015.



Experiments on fire smoke detection (Nov. 2014-Feb.2015).

Two records of ongoing laser pulse and two return pulses. 1 and 3 : two emitted pulses from a Nd :YAG (Brilliant B of Quantel) of pulse lengths 5.2 et 5.4 ns. 2 : return pulse from a solid target (wall) after 65 ns. 4 : the return pulse reflected by a weak smoke large of 24 cm at 5.2 m from the laser. Pulse 3 is scattered by the air close to the detector.



ATMRES, UKZN, Durban, 10 Sep. 2015

Pulse	1	2	3	4
Pulse length (ns)	3.6	13	8	6
Object position (m)/ongoing pulse	0	2.25	4.55	9.75
Nature of the object*	Ongoing pulse	Smoke wice of 1.1 m	Smoke wice of 36 cm	Wall hidden by the smoke and by curtain

* the nature of the object is recognized from the pulse broadening:

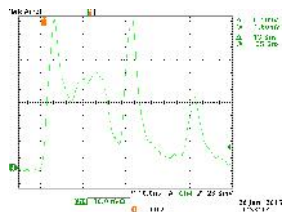
$$\Delta R = \frac{c \Delta t_p}{2} = \frac{c(t_p^2 - t_p^1)}{2}$$

ΔR : the object size.

Δt_p width difference between the ongoing and the return pulses. If $\Delta t_p / t_p \approx 0$ The return pulse reflects on a solid target.

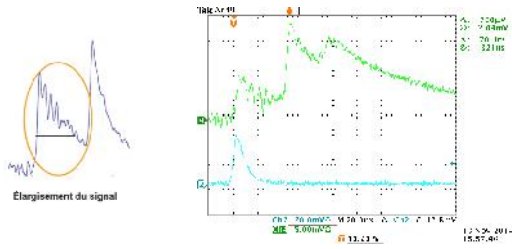
ATMRES, UKZN, Durban, 10 Sep. 2015

It is possible to recognise the smoke structure in this example

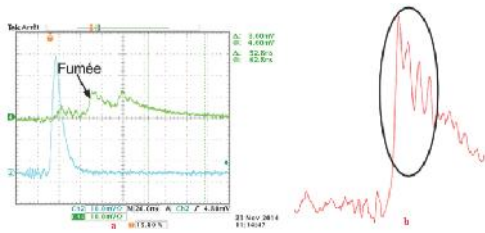


ATMRES, UKZN, Durban, 10 Sep. 2015

Isolation of the smoke signature on the return pulse.

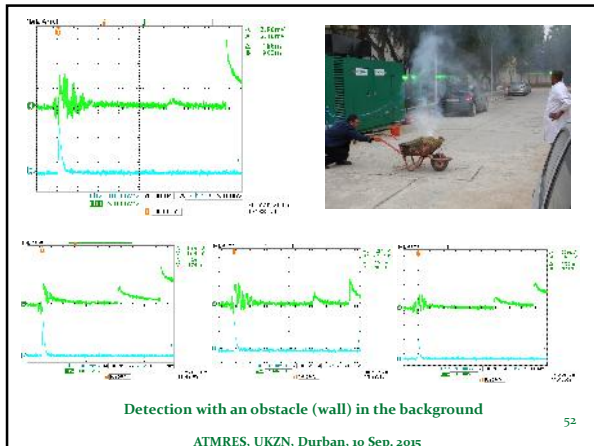


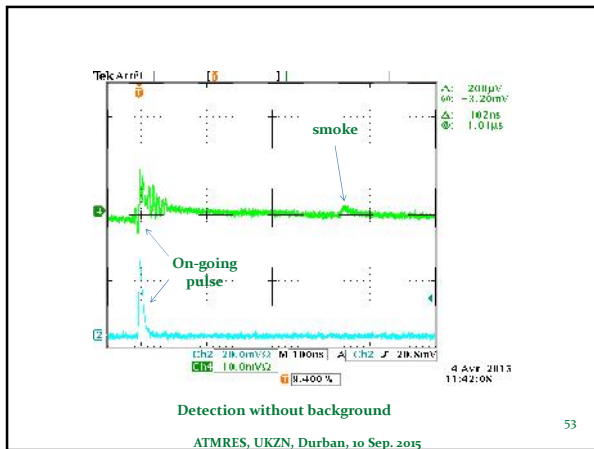
Isolation of the smoke signature on the return pulse.





Experiment in an extended area at CDTA.





VI- The saturation issue

ATMRES, UKZN, Durban, 10 Sep. 2015

La problématique de la détection

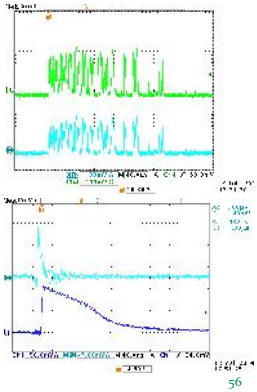
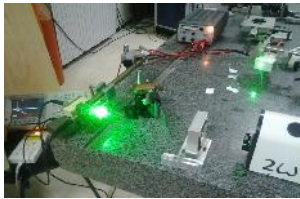


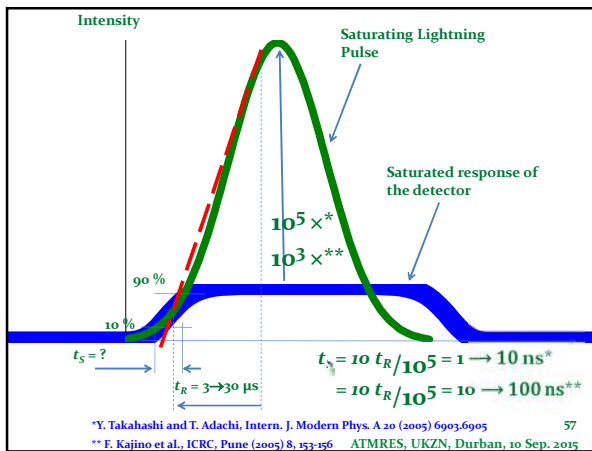
Fig. 1 - The two positions of interest for the photo-detection in remote sensing.

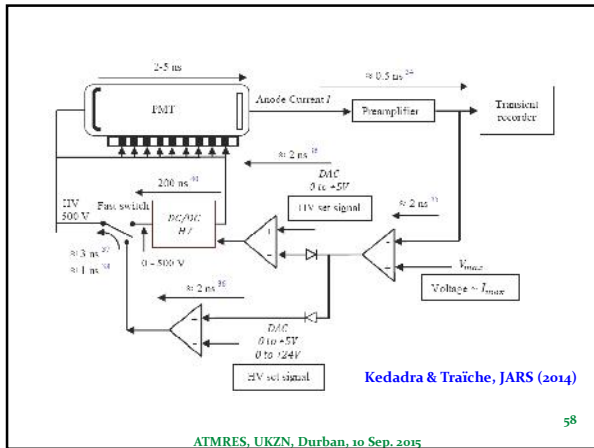
Kedadra & Traïche, JARS (2014)

Saturated signal at the output of a photodiode

To be avoided







Conclusion




The single pulse-based detection deserves more investigation regarding the physical phenomena it gives access to.

Thank you !

Laser based optical communication in free-space

Yaseera Ismail and Sharmini Pillay

Laser and Optics in Atmospheric Remote Sensing Workshop
Durban, South Africa
10-11 September 2015

Quantum Information Science

A study based on the idea that the manipulation of information is bound only by the laws of physics and thus information can be characterised, quantified and processed as a physical entity using the basic properties of quantum mechanics.

QUANTUM COMPUTING

Classical Bit

1 bit: 0 or 1

2 bits: 00, 01, 10, 11

Either 0 or 1

One out of 2ⁿ possible permutations

Quantum Bit

1 bit: 0 or 1

2 bits: 00, 01, 10, 11, 00, 01, 10, 11

Both 0 and 1

All of 2ⁿ possible permutations

QUANTUM COMMUNICATION


Alice

Qubit
 $\alpha|0\rangle + \beta|1\rangle$
 Photon

Bob

Quantum Communication deals with the transfer of information

Cryptography: The art of taking a message and rendering it unreadable to any unauthorised party



Sender (S) → Receiver (R)

MESSAGE (S to R)

FEEDBACK (R to S)

Sender: Clear text (Hello)

Encryption (using Recipient's public key)

Encrypted text (%f0sjh)

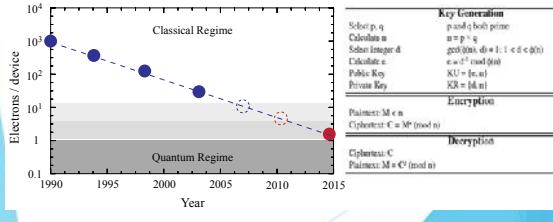
Decryption (using Recipient's private key)

Recipient: Clear text (Hello)

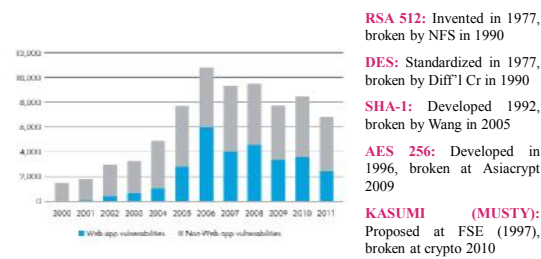
Classical Cryptography

Classical Cryptography

- Employs various **mathematical techniques** to restrict the eavesdropper from learning the content of the encrypted messages
- An absolute security of information is not guaranteed



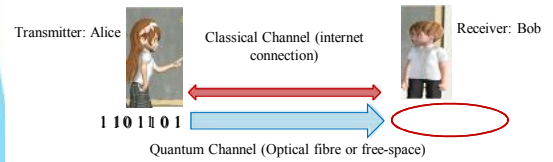
Vulnerabilities in the classical network year-by-year



Quantum Cryptography

Quantum Cryptography

- Information is protected by the **physical laws** of nature:
 - Heisenberg Uncertainty principle
 - No cloning theorem
- Provides a means for two parties to exchange information through a private channel with the complete security of communication



Requirements for the implementation of Quantum Key Distribution system

An appropriate encoding

- Polarisation
- Phase

Medium to transmit the single photons

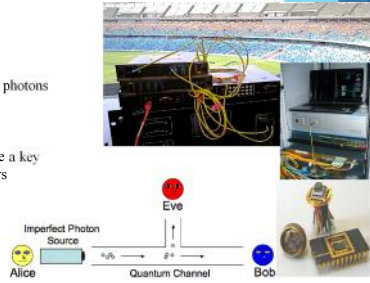
- Fibre
- Free-Space

A means to detect and generate a key

- Single photon detectors
- Classical Channel

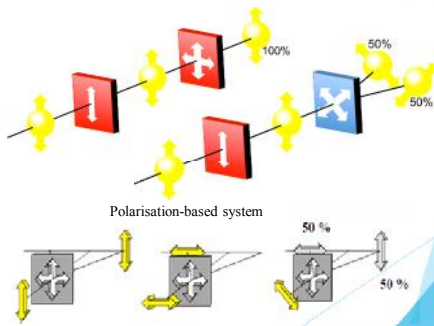
A single photon source

An appropriate protocol

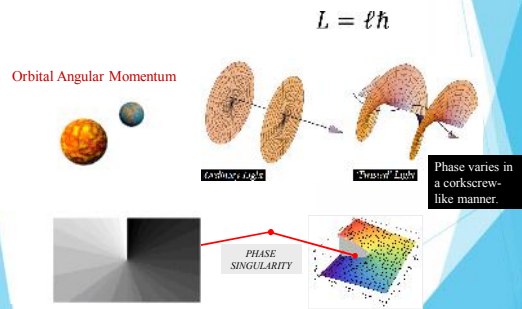


Method of Encoding (Polarisation or Phase)

Encoding using the state of polarisation

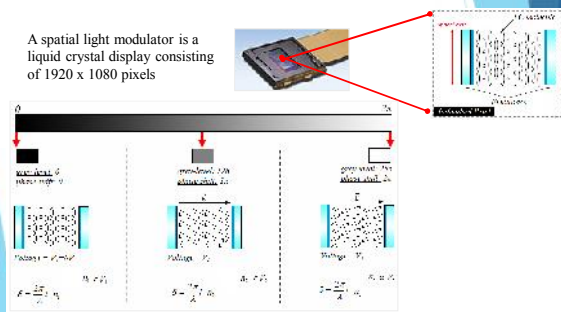


Light can be manipulated to carry Orbital Angular Momentum (OAM)

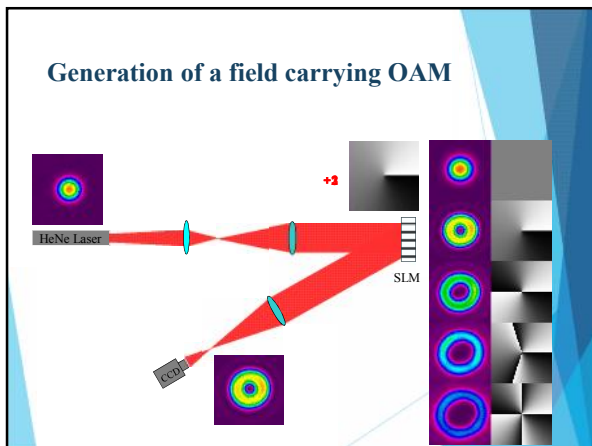


A spatial light modulator can be programmed to manipulate light

A spatial light modulator is a liquid crystal display consisting of 1920 x 1080 pixels

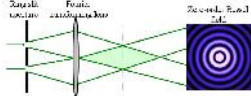


Generation of a field carrying OAM



Bessel beam can be manipulated to carry OAM

Durmin's Ring Slit Aperture Experiment:



$$T(\rho, \ell) = \text{Exp} \left[-2\pi \frac{\nu}{\rho_0} \right] \text{Exp} [i\ell \phi]$$

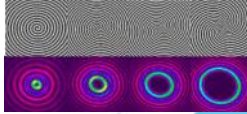
Order of the azimuthal index

J. Durmin, J.J. McIell and J.H. Eberly, Phys. Rev. Lett. 58 1499-1501 (1987).

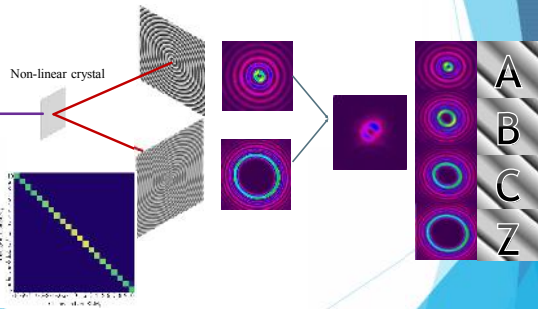
$$U(r, \theta) = A(r) J_\ell(k_r r) \text{Exp} \left[-i \left(\frac{r}{r_0} \right)^2 \right]$$

Bessel function

Gaussian beam

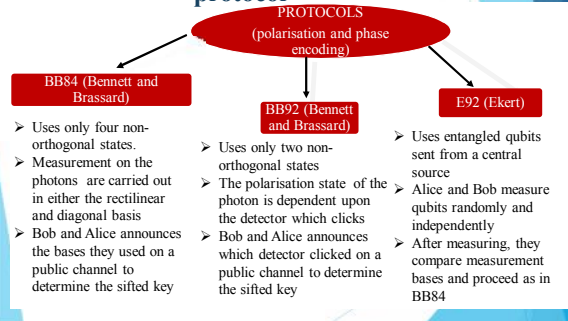


States carrying OAM results in dense coding

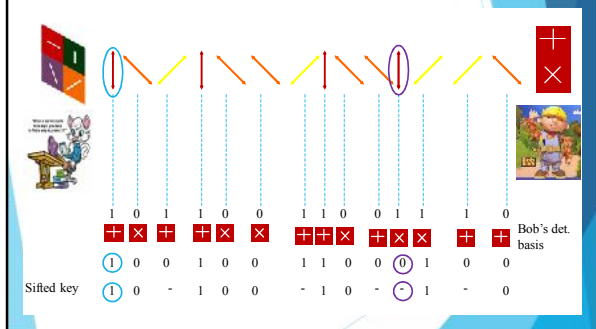


Quantum Key Distribution Protocols

The security of QKD lies on the implementation of an appropriate protocol

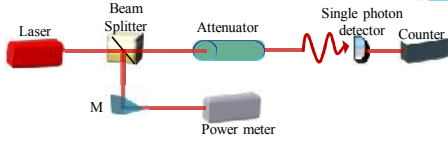


BB84 Protocol: The most fundamental protocol

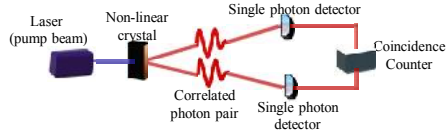


Single photon source

Generation of single photons as quantum carriers



Any attempt of eavesdropping will degrade the entanglement which can easily be detected

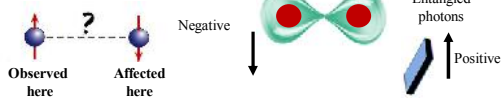


Generation of single photons as quantum carriers

- The wave-function of the particles cannot be separated:

$$|\Psi\rangle = \frac{1}{\sqrt{2}} (|00\rangle + |11\rangle)$$

- Measurement on one particle affects the state of the other

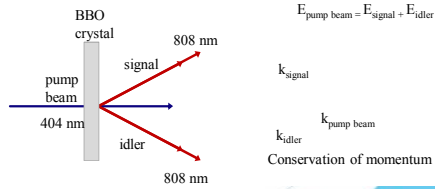


- There exist no classical model of this behaviour

"Spooky action at a distance"

During SPDC there is a conservation of energy and momentum

One particular method of obtaining entanglement is by pumping a non-linear crystal such that photons are split into a single photon pair known as the "signal" and the "idler."



Thank you



LASER AND OPTICS IN ATMOSPHERIC REMOTE SENSING - A TRAINING WORKSHOP
held at UKZN (Westville Campus, DURBAN, SOUTH AFRICA) on 10-11th September 2015



ATMOSPHERIC AEROSOL RETRIEVAL

using Sun-Photometer

Dr. Adesina Joseph

General outline

- Aerosols
- Key aerosols properties
- Sunphotometer a ground based instrument
- AERONET – Network of sunphotometer
- Sunphotometer Instrumentation

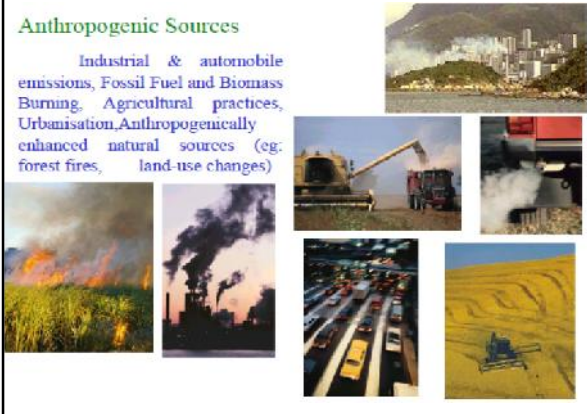
What are aerosols?

Earth's atmosphere consisting primarily of a mixture of gases also contains particles, such as aerosols and clouds. Aerosols are suspended liquid or solid particles whose typical diameters range over four orders of magnitude (sizes from ~ 3 nanometers, nm, to a few hundredths of millimeters, mm, generally smaller than cloud droplets) with a wide dynamic range of composition and shape, depending on their sources and atmospheric processes.

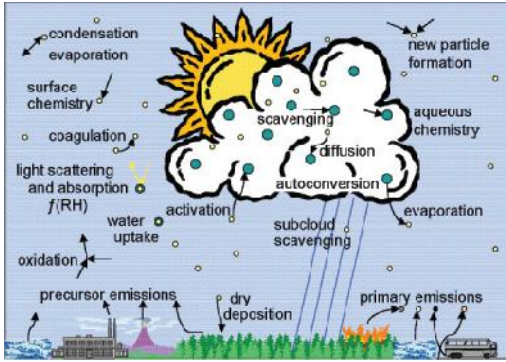
It is well known that aerosols can have a variety of important impacts on the environment. Aerosols, also known as particulate matter have long been recognized as pollutants of concern and may have detrimental effects on human health.

Anthropogenic Sources

Industrial & automobile emissions, Fossil Fuel and Biomass Burning, Agricultural practices, Urbanisation, Anthropogenically enhanced natural sources (eg: forest fires, land-use changes)

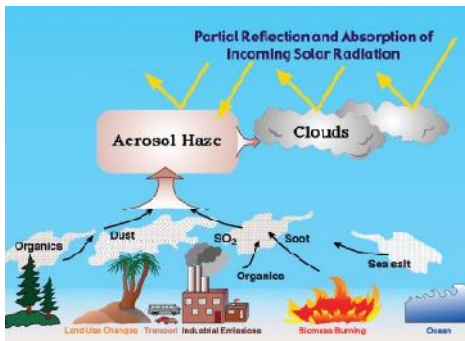


AEROSOLS IN THE ATMOSPHERE UNDERGO VARIOUS PROCESSES



From Ghan and Schwartz (2007).

AEROSOLS CLIMATE EFFECTS



BRIEF DESCRIPTION OF KEY AEROSOL, CLOUD, AND SURFACE PROPERTIES THAT DETERMINE THE AEROSOL RADIATIVE FORCING

• **Aerosol extinction coefficient:** Fraction of radiant flux lost from aerosol scattering and absorption per unit thickness of aerosol, with a unit of m^{-1} .

• **Aerosol Forcing:** of a quantity such as solar irradiance or flux is defined as the difference in the quantity with and without aerosols present. Sometimes aerosol forcing just refers to the industrial period in which case the forcing is the change in quantity calculated with aerosols present during the pre-industrial and industrial periods.

• **Aerosol optical depth (AOD):** a measure of aerosol amount in optical sense. It is an e-folding length of the decrease of a direct beam due to the extinction when traveling through the aerosol layer. Changes of AOD with wavelength are usually represented by the Angstrom exponent, with high values of Angstrom exponent indicative of small particles (industrial pollution and biomass burning smoke) and low values representative of large particles (mineral dust and sea-salt).

• **Aerosol mass extinction (scattering, absorption) efficiency:** the aerosol extinction (scattering, absorption) coefficient per unit aerosol mass concentration, with a unit of m^2g^{-1} .

• **Aerosol phase function:** a description of the angular distribution of scattering radiation. In practice, the phase function is parameterized with **asymmetry factor (g)**, with $g=1$ for completely forward scattering and $g=0$ for symmetric scattering. Another relevant parameter is the **hemispheric backscattered fraction (b)**, a fraction of the scattered intensity that is redirected into the backward hemisphere of the particle and can be derived from measurements made with an integrating nephelometer. The larger the particle size, the more the scattering in the forward hemisphere (i.e., larger g and smaller b).

• **Aerosol single-scattering albedo (SSA , ω_0):** a measure of relative importance of scattering and absorption. It is defined as a ratio of the scattering coefficient to the extinction coefficient. The smaller the SSA , the more absorbing the aerosol is.

• **Internal mixture vs external mixture:** Internal mixture is a chemically homogeneous mixture of particles in air, with each particle having about the same chemical composition. For external mixture, individual particles in the aerosol do not have the same chemical compositions or necessarily the same size distribution. The internal mixture has a higher absorption coefficient than the external mixture

• **Cloud condensation nuclei (CCN):** Aerosol particles that act as seeds for the formation of clouds through the condensation of water molecules onto their surfaces at low supersaturation. The activation of aerosol particles to CCN depends on the size and chemical composition of particles.

• **Cloud albedo:** Fraction of incident radiant flux reflected by cloud. The cloud albedo depends on the number and size of cloud droplets, and water path. In comparison to clean clouds, polluted clouds have more cloud droplet number and smaller droplet size and are more reflective (i.e., higher cloud albedo).

• **Surface albedo:** Fraction of incident radiant flux reflected by surface. It depends not only on surface type but also on geometry of incident light. In general, land has a larger albedo than ocean (glint-free conditions), and desert has a larger albedo than forest. The larger the surface albedo, the less negative the aerosol radiative effect at the TOA is. The TOA aerosol radiative effect can shift from negative (cooling) over ocean to positive (warming) over bright land, if aerosol is partly absorbing.

Surface remote sensing compare to satellite and in-situ measurements

Instrument	Advantages	Disadvantages
Ground-based remote sensing	<ul style="list-style-type: none">- high information on aerosol ($0^\circ \leq \Theta_{\text{view}} \leq 150^\circ$; transmitted light dominates over reflected);- non-intrusive measurements;- easy access to equipment;	<ul style="list-style-type: none">- local coverage;- limited vertical and backscattering information;- indirect measurements;- very limited capability in presence of clouds
Satellite remote sensing	<ul style="list-style-type: none">- global coverage;- non-intrusive measurements	<ul style="list-style-type: none">- limited on information aerosol ($45^\circ \leq \Theta_{\text{view}} \leq 150^\circ$; aerosol and surface effects to be separated);- no access to equipment
In-situ measurements	<ul style="list-style-type: none">- very straightforward;- unique aerosol physical and chemical information;- universal applicability- (e.g. in cloudy atmosphere);	<ul style="list-style-type: none">- intrusive measurements;- local coverage

What is the main strength of remote sensing from ground for characterization of aerosol and radiation ?

Because, it provides most accurate information regarding aerosol abilities to change atmospheric radiation, i.e. about:

- aerosol loading ($\tau(\lambda)$ - aerosol optical thickness);
- angular distribution of aerosol scattering ($P(\Theta;\lambda)$ - phase function);
- degree of aerosol absorption ($\omega_0(\lambda)$ -single scattering albedo)

Aerosol light scattering and absorption



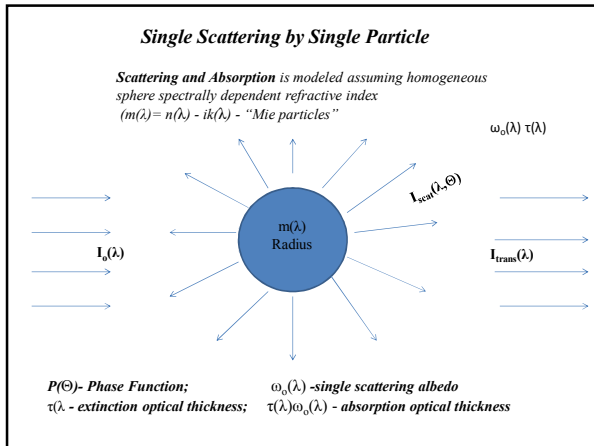
Scattering by large particles (aerosols, cloud droplets, shown here as a black dot) whose size d is approximately equal to λ , wavelength of light, is predominantly in the forward direction (red arrow).

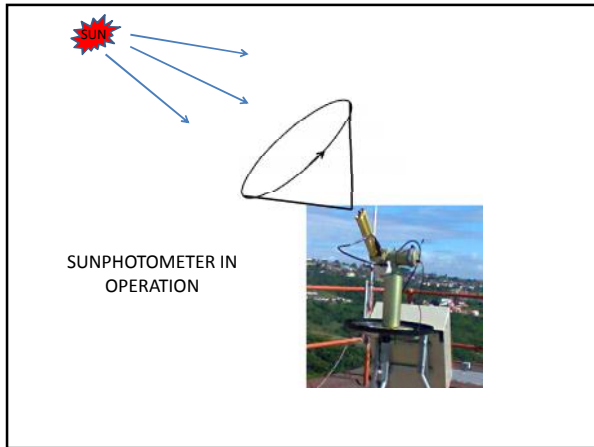


Particles with a large imaginary part of the refractive index have significant absorption

Aerosol (Mie) Scattering:
When particle sizes are large (comparable to the wavelength of light) the scattering cross-section (probability for scattering) increases dramatically. However there are many more molecules than particles in the atmosphere, with the result that the two effects are comparable.

Aerosol Absorption:
Particles made of sulfates and sea-salt do not absorb light at solar wavelengths. Soot particles (i.e., those that are black), absorb solar and terrestrial radiation. At those wavelengths, the complex refractive index of these particles has a significant imaginary component





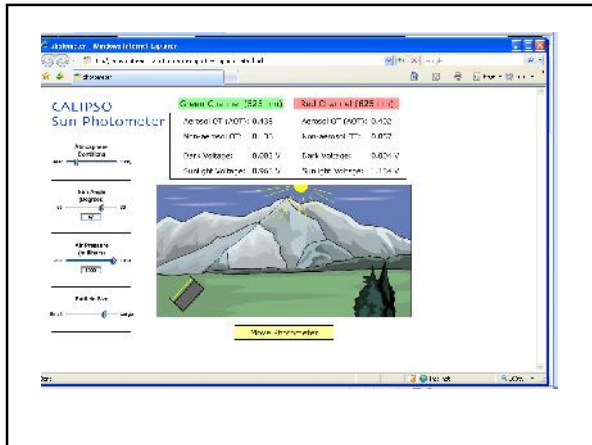
How does the Sun Photometer Work?

- Sun Photometers absorb *direct* sunlight energy with an LED light and convert the intensity into a quantified voltage to measure aerosols in the atmosphere.
- The intensity of sunlight at the top of the earth's atmosphere is constant. While the sunlight travels through the atmosphere, though, aerosols can dissipate the energy by scattering and absorbing the light. More aerosols in the atmosphere cause more scattering and less energy transmitted to the surface.
- Knowing the sunlight's energy at the top of the atmosphere, the thickness of the atmosphere, and the amount of sunlight transmitted to the earth's surface and can allow us to determine the amount of scattering, and thus, the amount of aerosols.

Sun Photometer Simulator

<http://calipsooutreach.hamptonu.edu/sunphoto-sim/sunphotometer.html>

- Click on LAUNCH
- You can vary sun angle, atmospheric pressure, haziness, and particle size to see impact on green channel and red channel sun voltage, and aerosol OD.



What each variation means

- **Atmospheric Conditions** - Level of haze due to aerosols.
- **Sun Angle (Degrees)** - (90 degrees is straight overhead) Decreased sun angle early and late in the day increases the amount of atmosphere that the light from the sun passes through before reaching sun photometer.
- **Air pressure** - Changes in air pressure (due to altitude or weather systems) change the density of the air. A decrease in air pressure (decrease in air density) causes less light to be scattered by air molecules and increases the amount of light reaching the sun photometer.
- **Particle size** - The relative scattering of red vs. green light by aerosol particles is dependent on the particle size.

Data Collection

- The Cimel Electronique 318A spectral radiometer is a solar-powered, weather-hardy, robotically-pointed sun and sky spectral sun photometer.
- A sensor head points the sensor head at the sun according to a preprogrammed routine.
- The Cimel controller, batteries, and Vitel satellite transmission equipment are usually deployed in a weatherproof plastic case.

- The radiometer makes two basic measurements-either direct sun or sky-both within several programmed sequences.
- The direct sun measurements are made in eight spectral bands requiring approximately 10 seconds
 - at wavelengths of 340, 380, 440, 500, 670, 870, 940 and 1020 nm
 - the 940 nm channel is used for column water abundance determination
- A preprogrammed sequence of measurements is taken by these instruments from 7 am-7pm daily.

- In addition to the direct solar irradiance measurements that are made with a field of view of 1.2 degrees, these instruments measure the sky radiance in four spectral bands (440, 670, 870 and 1020 nm) along the solar principal plane (i.e., at constant azimuth angle, with varied scattering angles) up to nine times a day and along the solar almucantar (i.e., at constant elevation angle, with varied azimuth angles) up to six times a day.
- The approach is to acquire aureole and sky radiances observations through a large range of scattering angles from the sun through a constant aerosol profile to retrieve size distribution, phase function and aerosol optical depth.

- During the large air mass periods direct sun measurements are made at 0.25 air mass intervals, while at smaller air masses the interval between measurements is typically 15 minutes. The time variation of clouds is usually greater than that of aerosols causing an observable variation in the triplets that can be used to screen clouds in many cases.
- Additionally the 15-minute interval allows a longer temporal frequency check for cloud contamination.

Data Transfer

- **Satellite**
 - Data are transmitted hourly or half hourly from the memory of the sun photometer microprocessor via the Data Collection Systems (DCS) to either of three geosynchronous satellites GOES, METEOSAT or GMS and then retransmitted to the appropriate ground receiving station.
- **Internet**
 - Data may be downloaded automatically from the Cimel sun photometer and stored on the local computer. This computer can run software to automatically transfer K7 files to the AERONET processing system through the Internet. Alternatively, users may download K7 files manually from the instruments using a PC or laptop and manually submit these files to the processing system.

What is AERONET?

- The AERONET (AErosol RObotic NETwork) program is a federation of ground-based remote sensing aerosol networks collaborated on by national agencies, institutes, universities, individual scientists, and partners.
- The program provides a long-term, continuous and readily accessible public domain database of aerosol optical depth, microphysical and radiative properties for aerosol research and characterization, validation of satellite retrievals, and synergism with other databases.

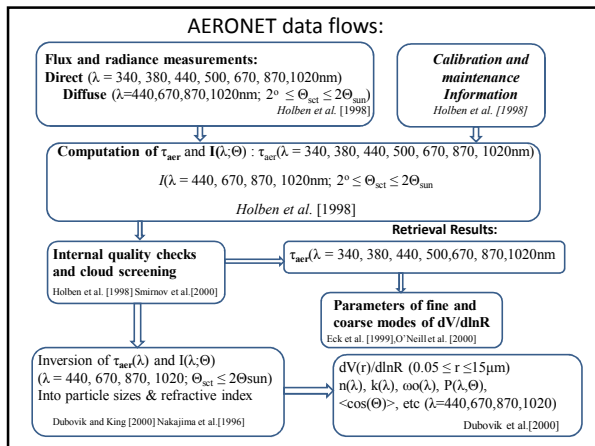
Data Processing and Access

- Once collected, AERONET data is post-processed with 4 algorithms
 - Aerosol Optical Depth (AOD) retrieval
 - AOD cloud screening
 - Sea-prism processing
 - Sky Radiance data (Almucantars and Principal Planes) inversion
- Then it is stored online and access is available to anyone

Data Types

- Aerosol Optical Depth (AOD)
 - Sun photometer measurements of the direct solar radiation provide information to calculate the columnar aerosol optical depth (AOD).
 - AOD can be used to compute columnar water vapor (Precipitable Water) and estimate the aerosol size.
- Aerosol Inversions
 - Inverting sun photometer radiance measurements produces aerosol optical properties such as size distribution, single scattering albedo, phase functions, and the complex index of refraction.
- Solar Flux
 - High frequency solar flux calculations. A companion to AERONET.

- Ocean Color
 - A new network component called AERONET – Ocean Color (AERONET-OC). Provides the additional capability of measuring the radiance emerging from the sea (i.e., water-leaving radiance) with modified sun-photometers installed on offshore platforms like lighthouses, oceanographic and oil towers.
 - AERONET-OC is instrumental in satellite ocean color validation activities through standardized measurements a) performed at different sites with a single measuring system and protocol, b) calibrated with an identical reference source and method, and c) processed with the same code.



Sensitivity to instrumental offsets
Offsets were considered in:

- optical thickness: $\Delta\tau(\lambda) = \pm 0.01; \pm 0.02;$
- sky-channel calibration: $\Delta I(\lambda; \Theta) / I(\lambda; \Theta) 100\% = \pm 5\%;$
- azimuth angle pointing: $\Delta\phi = 0.5^\circ; 1^\circ$
- assumed ground reflectance: $\Delta A(\lambda) / A(\lambda) 100\% = \pm 30\%; \pm 50\%;$

Aerosol models considered (bi - modal log-normal):

- Water-soluble aerosol for $0.05 \leq \tau(440) \leq 1;$
- Desert dust for $0.5 \leq \tau(440) \leq 1;$
- Biomass burning for $0.5 \leq \tau(440) \leq 1;$

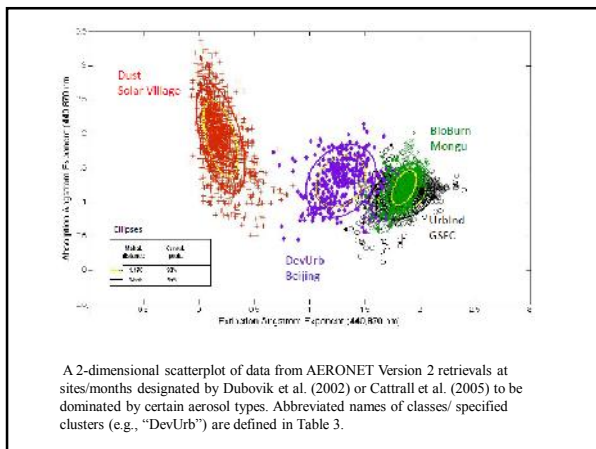
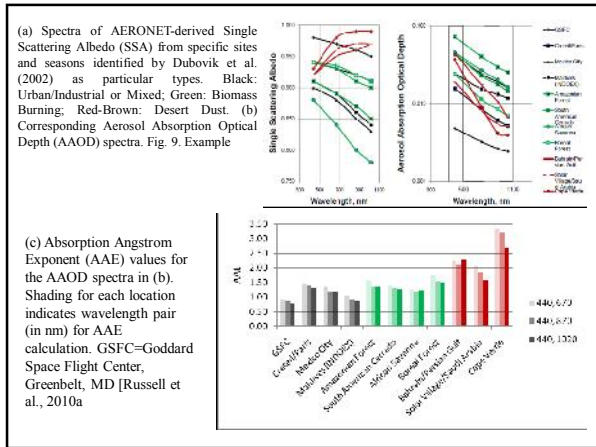
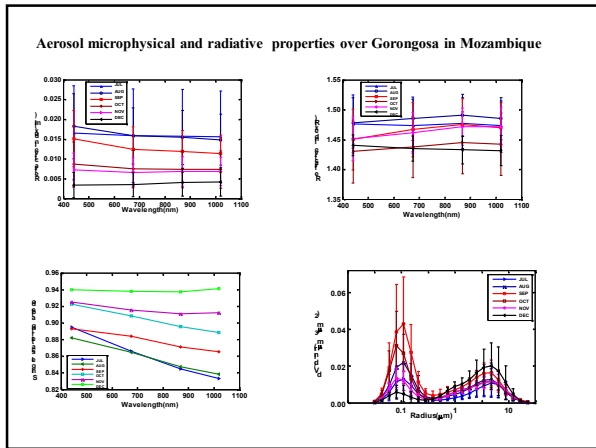
Results summary:

- $\tau(440) \leq 0.2$ - dV/dlnr (+), n(λ) (-), k(λ) (-), (λ) ω₀ (-)
- $\tau(440) > 0.2$ - dV/dlnr (+), n(λ) (+), k(λ) (+), ω₀ (λ) (+)
- Angular pointing accuracy is critical for dV/dlnr of dust

(+) **CAN BE** retrieved (-) **CAN NOT BE** retrieved

Products of AERONET inversions

- **Microphysics (columnar aerosol):**
dV(r)/dlnr - volume (number, area, etc.) particle size distribution ($0.05 \mu\text{m} \leq r \leq 15 \mu\text{m}$)
- **Standard Parameters of dV(r)/dlnr**
c_v - volume concentration (t, f, c);
r_v - volume median radius (t, f, c);
σ - standard deviation (t, f, c);
r_{eff} - effective radius (t, f, c);
(t - total aerosol, f - fine and c - coarse modes)
n(λ) - ($1.33 \leq n(\lambda) \leq 1.6$)
k(λ) - ($0.0005 \leq k(\lambda) \leq 0.5$)
- **Radiative properties:**
ω₀(λ) - Single Scattering Albedo
P(Θ; λ) - Phase function (t, f, c);
τ(λ) - Optical thickness (f, c);
F(λ) - Direct and diffuse fluxes



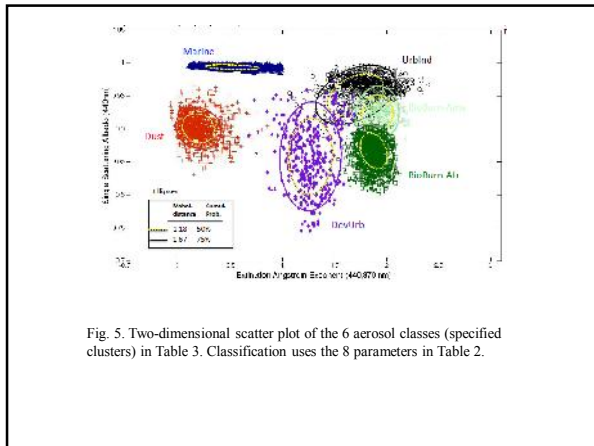


Fig. 5. Two-dimensional scatter plot of the 6 aerosol classes (specified clusters) in Table 3. Classification uses the 8 parameters in Table 2.

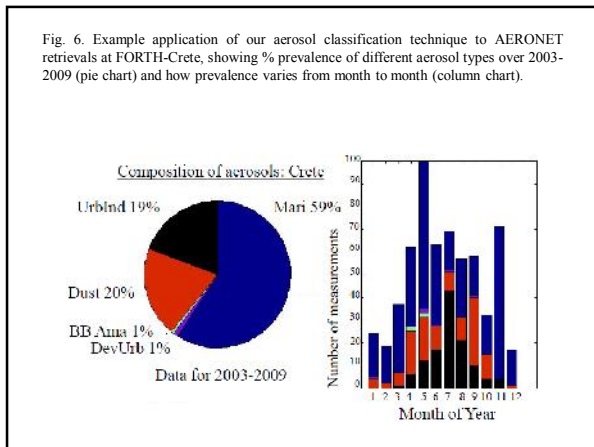


Fig. 6. Example application of our aerosol classification technique to AERONET retrievals at FORTH-Crete, showing % prevalence of different aerosol types over 2003-2009 (pie chart) and how prevalence varies from month to month (column chart).

Class Assignment

- Using AOD data from Pretoria_CSIR-DPSS
 - Data Download Process
 - Data Analysis Tips
 - Assignment

- Possible answers to assignment

Data Collection

- AERONET collaboration provides globally distributed observations of
 - spectral aerosol optical depth (AOD)
 - inversions
 - precipitable water
- The network imposes standardization of instruments, calibration, processing and distribution.
- Aerosol optical depth data are computed for three data quality levels:
 - Level 1.0 (unscreened)
 - Level 1.5 (cloud-screened)
 - Level 2.0 (cloud screened and quality-assured)

Data Retrieval

- We will be using data from January 2012 from the [Pretoria CSIR-DPSS](#)
- In left column, click on **Download Tool** under **Aerosol Optical Depth**
- Then click on [Pretoria CSIR-DPSS \(25S,28E\)](#) under the map

- Version 2 Direct Sun Algorithm
- Start Date
1 Jan 2012
- End Date
31 Dec 2012
- Choose **Level 2.0** for AOD w/
Precipitable Water
- Choose **Single File** for Instrument
Information
- Choose **Level 2.0** for Total Optical
Depth
- Choose **Level 1.5** for AOD Mode
- Choose **Daily Ave** for Data Form

You should be on a page that looks like this

Station ID	Station Name	Date Range
25S,28E	Pretoria CSIR-DPSS (25S,28E)	2012-01-01 to 2012-12-31

Saving Data

- Click Download
- Accept Conditions
- Save .zip file as 120101_121231_Pretoria_CSIR_DPSS

Opening Data

- Use a file extractor to unzip files
 - In Windows, simply right click on zipped folder, choose **Extract All**, and go through the Extraction Wizard. This will create a new folder with the 4 unzipped files. (If you still need help, check out the Data File Help Page at http://aeronet.gsfc.nasa.gov/new_web/file_help.html).
 - Once files have been unzipped, open a spreadsheet program (i.e. MS Excel). Go to **File** and **Open**. Choose the **LEV20** file (you may have to change type to all files to see them).
 - Choose **Delimited** as your data type, then **Comma** (or **tab** if columns don't show up when you scroll down) as your delimiter.
 - Make sure the first column is in **Date Format (DMY)**- this will work with Tot20 file, not other 2)

Data Management

- If you repeat with each data file you should have 4 in total: Lev20, Oneil_15, Sloar_Info and Excel (Tot20)
- Save each file as an Excel Workbook
- For help with column header meaning and units, visit http://aeronet.gsfc.nasa.gov/new_web/units.html

Apr 23 at 7:28:30 AM

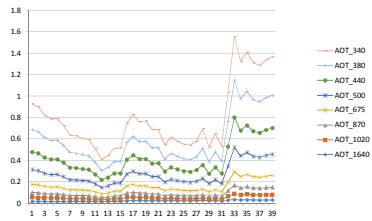
31 (Jan)+28 (Feb)+31 (Mar)+23 (Apr)=113
Convert 7 hrs into seconds: $7*60*60=25200$
 $25200+28*60=26880+30=26910$

$26910/86400$ seconds in a day=.3114583

113.3114583

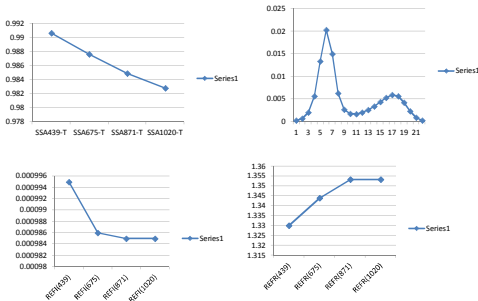
• Part 2: Data Analysis

- Using the Lev20 file, plot the total AOD for each wavelength by JD for the first day all on the same plot. What do you notice? (**the smaller wavelengths see higher optical depths**). Why do you think this is? (**Aerosol optical depths typically decrease with increasing wavelength**). What else can you see? (**AOD increased towards evening**)



• Part 3: Data Analysis

- Using the Dubovik file, plot the SSA, Volume size distribution (VSD), Refractive Index real and imaginary.

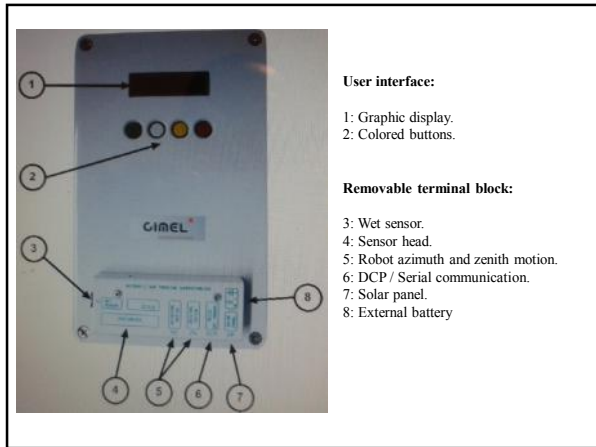


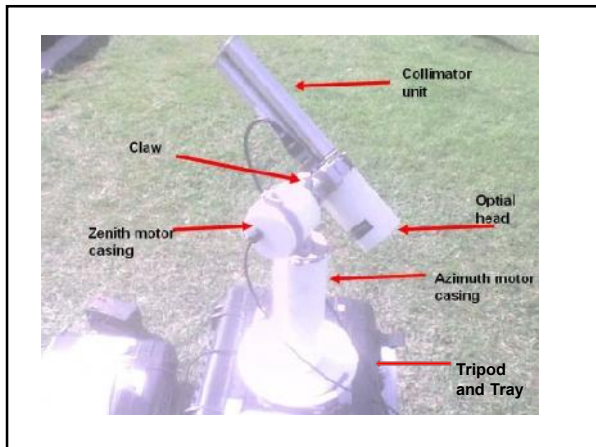
Instrumentation

1. The Control Unit (CU)

The Control Unit is on one hand the component where all the data acquired by the optical head are sent and on the other hand is used as the user interface to parameterize the whole system running.

The CU gets four keys, a yellow push button and a screen display which enable the users to navigate through the menus.





2. Sensor (Optical) head

The sensor head measures the received signal from the sun, sky, soil or sea. Then it is sent and recorded to the CU.

Detectors can be either silicon and InGaAs or silicon only for the SEAPRISM sensor head. InGaAs detector is used for near-infrared wavelengths.

3. Collimator

The collimator is a component that enables the light to be guided correctly to the outside lenses on the sensor head. The collimator helps to reduce the stray light.

4. Robot

The robot is the component on which the sensor head is attached. Its mechanical design enables it to point on whole directions of the sky on the azimuthal and zenithal angles with a very high accuracy.

5. Tripod and tray

The tripod is the supplied infrastructure where the protection case and the robot are fixed and that enables the whole system to be stably fixed on the ground.

The tray is a part fixed horizontally on the tripod and where the robot will be fixed on.

How to enable the automatic mode

How to enable the automatic mode (applicable only for the screen 2 with initial location "Ready" state)

Step 1: Turn the power on (PW) (initially OFF)

- Send
- confirmation

Step 2: Select the power mode (PW)

Step 3: Toggle the parameter on a value of "1" (PW)

Step 4: Send the power mode (PW)

Step 5: Toggle the parameter on a value of "YES"

000400	0722
PW MAN SEL	Y/N
072600	PW 0
Param Word	- 1
072600	PW 1
Param Word	-
072700	
BTN ON DAY PAR	
ANS	NO
OK X	-
072700	
BTN ON DAY PAR	
ANS	YES
OK X	-
Valid Y	
NO	YES

How to disable the automatic mode

Step 1: Select the power mode (PW)

Step 2: Toggle the parameter on a value of "0" (PW)

Step 3: Send the parameter (PW)

Step 4: Toggle the parameter on (PW)

Step 5: Send the parameter (PW)

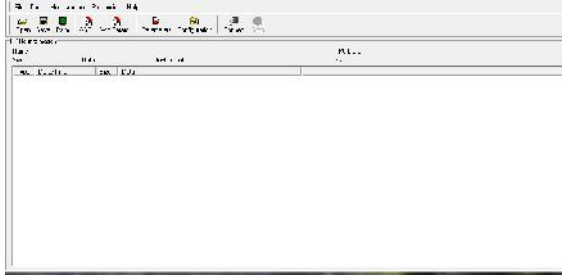
Step 6: Toggle the parameter on (PW)

Step 7: Send the parameter (PW)

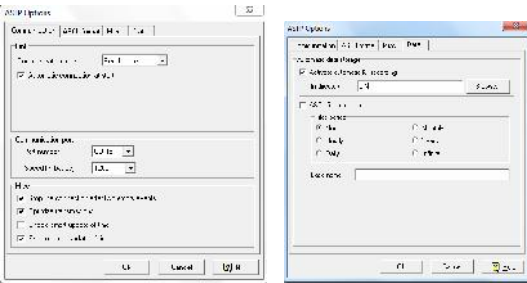
072600	PW 0
Param Word	-
072600	PW 1
Param Word	- 1
072700	
BTN ON DAY PAR	
ANS	YES
OK X	- 1
072700	
BTN ON DAY PAR	
ANS	NO
OK X	- 1
Valid Y	
NO	YES
072700	
BTN ON DAY PAR	

Install ASTPWin on the computer

When the computer is connected to the Sunphotometer then data can be downloaded and the software creates a k7 file. It can also create an ASCII file. The unprocessed data is the level 1.0, when it is cloud screened then it becomes level 1.5. The final processing gives the quality assured data.



How to configure ASTPWin



Sources

1. AERONET: An Introductory Lesson and Class - Shaunna Donaher
2. Inversion of Sun & Sky Radiance to Derive Aerosol Properties from AERONET - Oleg Dubovik
3. Aerosol Classification Using Multi-parameter Retrievals from Remote Measurements on Space and Other Platforms - P. Russell, M. Kacenenbogen, P. Hamill, J. Livingston, S. Burton, G. Schuster, O. Hasekamp, K. Knobelspiesse, Y. Shinozuka, J. Redemann, S. Ramachandran, B. Holben.
4. Aerosol Climatology and its importance - R. Ramakrishna Reddy (SASAS 2013)
5. Aerosol properties and their impact on climate - L. Remer, M. Chin, P. L. DeCola, G. Feingold, R. N. Halthore, P. Quinn, D. Rind, S. E. Schwartz, D. G. Streets, H. Yu.

Lecture Material

Solar Radiometry

Chapter 1: Introduction to Radiometry

- 1.1 Radiometric definitions
 - 1.1.1 Radiant flux
 - 1.1.2 Irradiance
 - 1.1.3 Radiance existence
 - 1.1.4 Radiant exposure
- 1.2 Why is light measured?
- 1.3 A brief radiometry history
- 1.4 Radiometric measurement process
- 1.5 Applications of radiometry

Chapter 2: Radiometric Approximations

- 2.1 Inverse square law
- 2.2 Cosine law
- 2.3 Lambertian Approximation

Chapter 3: Solar Radiometry

- 3.1 Solar radiation fundamentals
- 3.2 Solar angles
- 3.3 Components of solar radiation
- 3.4 Solar radiometry instrumentation
- 3.5 Solar radiometry station

Chapter 1: Introduction to Radiometry

Radiometry is the science and technology of the measurement of electromagnetic radiant energy. Measurements of radiant energy are conducted throughout the electromagnetic spectrum, as shown in figures 1.1 and 1.2, using methods which are suited to the spectral region of interest [1].

The optical radiation spectrum includes the ultraviolet (UV), visible (VIS), and infrared (IR) regions (shown in figures 1.1 and 1.2.). The visible portion of the optical spectrum covers a rather narrow band of wavelengths between 380 nm and 760 nm; the radiation between these limits, perceivable by the unaided normal human eye, is termed "light." Measurements within this region may be called "photometric" if the instruments used incorporate the response of the eye. The short wavelength (ultraviolet) limit of radiometric coverage is about 200 nm, approximately the shortest wavelength that our atmosphere will transmit. The longest wavelength (infrared) is about 100 μm . This wavelength range includes 99% of the energy (95% of the photons) from a thermal radiator at 0° C (273.16 K) [2].

Typical *sources* of radiant energy include the sun, lasers, electrical discharge sources, fluorescent materials, and in general any material body which is heated to a temperature above absolute zero. *Optical systems* used in radiometric measurement systems will usually consist of lenses, mirrors, apertures, prisms, gratings, filters, interferometers, polarizers, attenuators, diffusers, integrating spheres, fiber optics, or other devices [2].

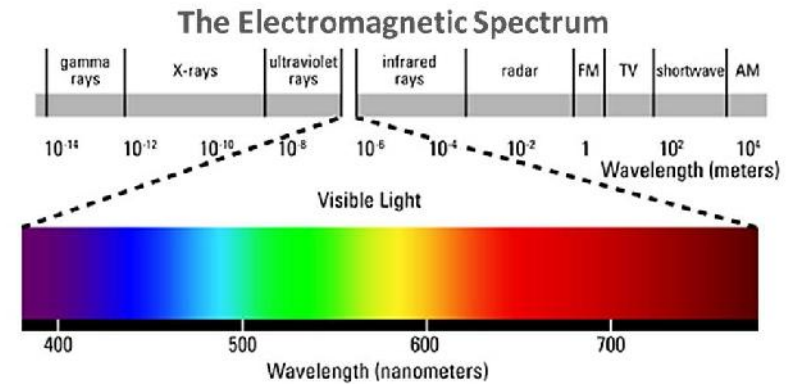


Figure 1.1: Electromagnetic Spectrum [3].

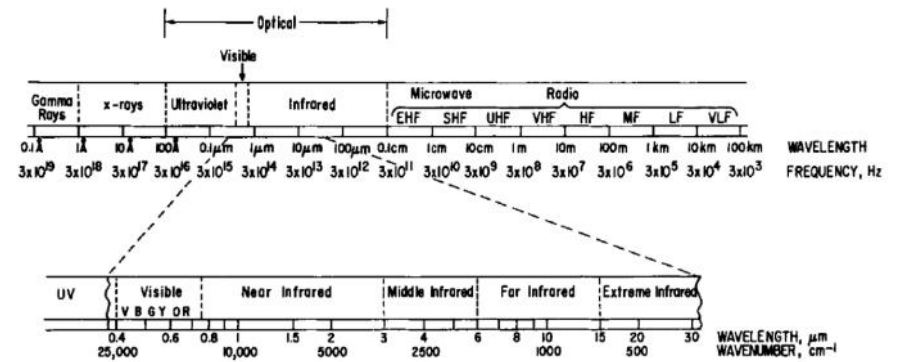


Figure 1.2: Electromagnetic Spectrum with further detail on the infrared region [1].

1.1 Radiometric definitions

Radio: meaning ray, ray-like.

-metry: meaning the process, art, or science of measuring

Radiometry: the use of the radiometer: the measurement of radiation.

Radiometer: [*radio-* + *-meter*], an instrument for detecting and measuring the intensity of radiant energy [2].

1.1.1 Radiant flux (W): the power emitted or received in the form of radiation.

1.1.2 Irradiance (W/m^2): the radiant power or the radiant flux incident per unit area of a surface.

1.1.3 Radiant exitance (W/m^2): the amount of radiation or radiant flux exiting a surface of unit area.

1.1.4 Radiant exposure (J/m^2): the quantity of radiation or radiant flux received by a unit of a surface over a time interval [4].

1.2 Why is light measured?

The measurement of light is often critical in transitioning from theory to the development of systems and techniques. Although instrument and system design may be based on theory, performance evaluation and system improvement require that accurate radiometric measurements be applied. When calibrated measurements are needed, that is, when field or laboratory measurements must be correlated with specific values presenting the relationship between measured phenomena and an absolute standard, radiometric measurements take on even greater significance [2].

1.3 A brief radiometry history

The most primitive beginnings of radiometry must have been the observation by early man of the different brightnesses of stars and the sensing of the warmth from the sun and the fire (after he invented or discovered it). These were radiometric measurements, but they surely were not quantitative. Greek astronomers, especially Ptolemy and Hipparchus, made good estimates of star magnitudes, and these were extended by Galileo. These constituted the qualitative radiometry measurements [5].

Regarding quantitative radiometry, scientists and engineers have been involved in the measurement of light since the early experiments and instruments described by P. Bouguer in 1729 and by J. H. Lambert in 1760. Exploration into other spectral regions began with the discovery of the infrared region by W. Herschel in 1800 and the ultraviolet region by J. W. Ritter the following year. Table 1.1 shows some of the significant events in the history of radiometry and photometry [2].

1.4 Radiometric measurement process

In order to fully appreciate a radiometric measurement we must understand the processes of generation, transmission, and detection of optical radiation. A typical radiometric configuration is shown in figure 1.3.

A target, or object of measurement interest, can be either active, emitting radiation by virtue of its temperature or some form of atomic excitation, or passive, reflecting radiation from a different active or passive illuminator. Examples of active sources include the sun, tungsten or fluorescent lamps, lasers, and any nontransparent object with a temperature greater than 0 K. Passive sources include the entire range of natural and artificial reflective surfaces that make up our environment. An additional source of optical radiation can be classified as background, the radiation that maybe in our instrumental field of view along with the target. Also included is the intervening medium, the atmosphere, which includes both radiation sources and sinks, acting through the mechanisms of absorption, emission, and scattering. The small arrows in figure 1.3 represent scattered, absorbed, emitted, and reflected radiation. After traversing the atmosphere, the rays from the target (and possibly the background as well) reach our instrument, whose parameters

define the ranges, and over which the spatial, spectral, temporal, and radiometric characteristics of incoming radiation will be accepted. This is accomplished through the use of lenses and mirrors, choppers and apertures, prisms, gratings, filters, attenuators, polarizers, optical fibers etc. The optical radiation transmitted through the instrument is finally incident on one or an array of detectors. Detectors may be thermal (thermoelectric, bolometric, and pyroelectric) or photon (photoemissive, photoconductive, and photovoltaic) in character; other viable detectors include the human eye and photographic film. The final block in the diagram involves signal processing. Most of the detectors in common use generate electrical signals. Post-detector processing may include filtering, linearization, and background suppression before the processed result is recorded and displayed. Even the eye and film detectors include processing steps, such as the filtering and interpretation of information by the brain and the photographic development process for film [2].

1.5 Applications

There exists many different applications of radiometry that are of fundamental importance in an extremely wide range of applications. Some of these are listed below [2]:

- | | |
|----------------------------------|---------------------------|
| Astrophysics | Atmospheric physics |
| Clinical and diagnostic medicine | Remote-sensing satellites |
| Electro-optics | Illumination engineering |
| Laser measurements | Materials science |
| Meteorology | Military systems |
| Night-vision devices | Optoelectronics |
| Photobiology | Photochemistry |
| Photometry | Radiative heat transfer |
| Solar energy | Television systems. |

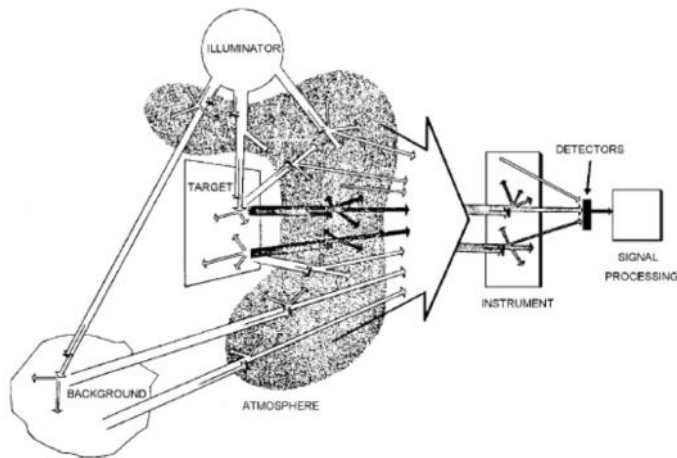


Figure 1.3: Illustration of a radiometric measurement setup [2].

Chapter 2: Radiometric Approximation

2.1 Inverse square law

The inverse square law of irradiance is a well-known approximation. The law states that the irradiance from an isotropic point source varies inversely with the square of the distance from the source. Figure 2.1 is used to illustrate the inverse square law. As shown in this figure, the rays are straight lines diverging from a source having an intensity I . At distance d , they fill area A . At a distance $2d$, the length of each side has doubled and the area subtended has increased by a factor of four. Assuming a lossless medium, the amount of radiant power at the second surface is the same as that at the first surface, due to the conservation of power. At this second surface, power is spread over a larger area, and irradiance decreases. The relationship between irradiance and distance is given by the following equation

$$E = \frac{I}{d^2}.$$

The above equation is specifically for the case where the area is perpendicular to the optical axis. For the case where the surface is tilted at an angle θ to the optical axis, an additional factor of $\cos \theta$ must be added:

$$E = \frac{I \cos \theta}{d^2} [2].$$

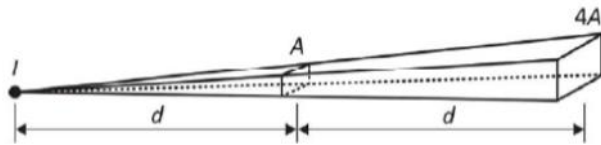


Figure 2.1: Illustration of the inverse square law [2].

2.2 Cosine³ law

The *Cosine³* law is applied to calculate the irradiance on a plane surface from an anisotropic point source. As depicted in Figure 2.2, the irradiance at a point x directly below the source with intensity I may be calculated according to the inverse square law as

$$E_x = \frac{I}{d^2}.$$

At position y , the distance from the source has increased such that $d = D / \cos \theta$. If the target at y is perpendicular to the vector between source and target, the irradiance at y is given by

$$E_y = \frac{I}{d^2} = \frac{I \cos^3 \theta}{D^2}.$$

If the target is now rotated so that it is parallel to surface x - y (the floor), an additional $\cos(\theta)$ term is introduced, which gives the following

$$E_y = \frac{I \cos^3 \theta}{D^2},$$

which is referred to as the *cosine³* law [2].

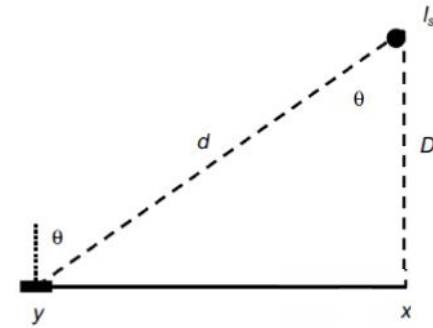


Figure 2.2: Illustration of the cosine³ law [2].

Table 1: Brief history of Radiometry

Year	Event	Principal investigator
?	... and then there was light!	from <i>Genesis</i>
1666	Investigation of the visible spectrum	Newton
1729	Inverse square law	Bouguer
1760	Cosine law, exponential absorption	Lambert
1800	Discovery of the infrared region	Herschel
1801	Discovery of the ultraviolet region	Ritter
1830	Radiation thermopile (first practical detector)	Nobile, Melloni
1837	Calorimetric detector	Pouillet
1839	Photoelectric effect	Becquerel
1859	Relation between absorption and emission	Kirchhoff

Year	Event	Principal investigator
1860	Standard lamp fueled by sperm whale oil	British Metropolitan Gas Act
1879	Incandescent lamp (carbon filament)	Edison
1880	Bolometer	Langley
1892	Integrating sphere (theory)	Sumner
1893	Absolute thermal detector (pyrheliometer)	Angstrom, Kurlbaum
1900	Blackbody radiation theory	Planck
1900	Integrating sphere (reduction to practice)	Ulbricht
1905	Photoelectric effect	Einstein
1910	Tungsten lamp	Collidge
1931	Adoption of colorimetric standards	International Commission on Illumination (CIE)
1936	Photomultiplier tube (multistage)	Zworykin, Morton & Malter
1938	Pyroelectric detector (theoretical)	Ta
1948	Adoption of platinum blackbody for standard candela	Consultative Committee on Photometry and Radiometry (CCPM)
1954	Silicon photodiode	Chapin, Fuller & Pearson
1955	Pyroelectric detector (reduction to practice)	Chenoweth
1960	Invention of light amplification by stimulated emission of radiation (LASER)	Maiman
1961	Tungsten-halogen lamp	Zubler & Mosby
1970	Laser calorimetry	West
1975	Fourier transform spectrometer	Vanesse
1977	Photometry relegated to subset of radiometry	CCPM
1980	Self-calibrated silicon detector	Zalewski & Geist
1983	Trap detector	Zalewski & Duda
1984	Definitive measurement of the Stefan-Boltzmann constant	Quinn & Martin
1985	Cryogenic absolute radiometer	Martin, Fox, & Key; Foukal

Chapter 3: Solar Radiometry

Solar radiation data at ground level are important for a wide range of applications in meteorology, engineering, agricultural sciences (particularly for soil physics, agricultural hydrology, crop modeling and estimating crop evapo-transpiration), as well as in the health sector (monitoring UV radiation levels) and in research in many fields of the natural sciences. A few examples showing the diversity of applications may include: architecture and building design (e.g. air conditioning and cooling systems); solar heating system design and use; solar power generation, weather and climate prediction models; evaporation and irrigation; calculation of water requirements for crops; monitoring plant growth and disease control and skin cancer research.

The solar radiation reaching the Earth upper atmosphere is a quantity rather constant in time. But the radiation reaching some point on Earth surface is random in nature, due to the gases, clouds and dust within the atmosphere, which absorb and/or scatter radiation at different wavelengths. Obtaining reliable radiation data at ground level requires systematic measurements.

The need for solar radiation data became more and more important mainly as a result of the increasing number of solar energy applications such as solar water heating, photovoltaic systems and concentrating solar powered systems [6].

3.1 Solar radiation fundamentals

The solar radiation emitted from the sun is in the form of electromagnetic energy. The radiation has wavelengths, λ , ranging from 300 (gamma rays) to 3000 nm (microwaves). Most of these wavelengths are screened from the earth's surface by different layers of the atmosphere. The main wavelength that does reach the surface is that of visible light ($380 < \lambda < 780$ nm). However, portions on either side of the visible spectrum are not completely cut off and are able to pass through the atmosphere. These are the ultra-violet ($\lambda < 380$ nm) and infrared ($\lambda > 780$ nm) ranges. The infrared range has wavelengths which are too long to be seen by the naked eye, whereas the ultra-violet region contains wavelengths which are too short. The solar spectrum is approximately equal to that of a black body at a temperature of 5800 K. Due to

the absorption of certain frequencies by water vapour, dust particles and other molecules in the air, the spectrum that is received by the earth's surface is significantly altered [7]. Figure 3.1 shows the solar energy spectrum.

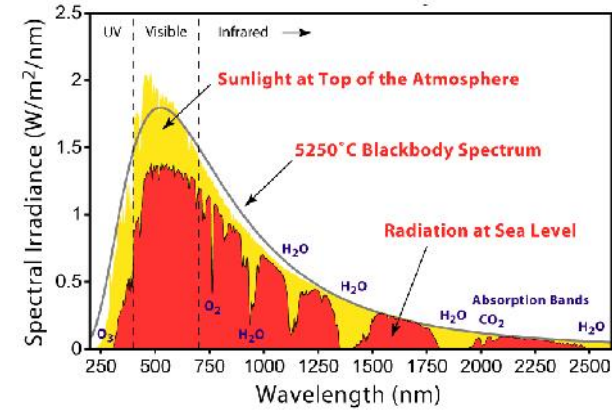


Figure 3.1: Solar energy spectrum [7].

The elliptical orbit of the earth's path around the sun is shown in figure 3.2. It indicates the position of the earth relative to the sun at different times of the year. The declination, δ , angle is the angle between the sun's direction and the equatorial plane. This angle varies through the year and is at its extreme during the solstices (longest or shortest length of day) and at zero during the equinoxes (equal day and equal night). The North-South (N-S) pole axis is normal to the equatorial plane whilst the declination axis is at an angle of $\delta_o = 23.45^\circ$ away from the normal to the plane of revolution [7].

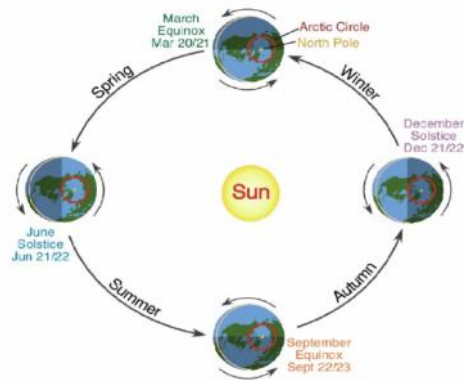


Figure 3.2: Sun-Earth geometry [8].

The variation of the declination angle is shown in figure 3.3 can be expressed by

$$\delta = \delta_o = \sin\left(\frac{360^\circ(284+n)}{365}\right),$$

where δ_o varies between $+\delta_o = +23.45^\circ$ (for mid-summer in the northern hemisphere) and $\delta_o = -23.45^\circ$ (for mid-winter in the northern hemisphere). The day in the year is represented by n where $n = 1$ for 1 January [7,9].

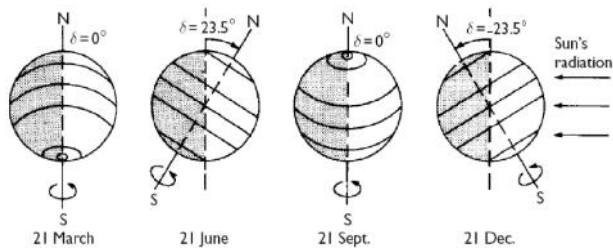


Figure 3.3: Variation of the declination angle through the year. The earth's circles of latitude are shown. A declination angle of 0° denotes the two equinoxes [9].

For solar energy calculations, apparent solar time (ST) is used to express the time of day. Apparent solar time is based on the apparent angular motion of the sun across the sky and does not coincide with clock time. The time when the sun crosses the meridian of the observer is the local solar noon. The relationship between apparent solar time and local standard time (LST) is calculated using the following equation

$$ST = LST + EOT + (l_{st} - l_{local}) \cdot 4 \text{ min/degree},$$

Where l_{st} and l_{local} is the standard meridian of the local time zone and local longitude, respectively and EOT is time in minutes given by

$$EOT = 9.87 \sin 2B - 7.53 \cos B - 1.5 \sin B,$$

where $B = 360(n-1)/364$ degrees [7,9].

3.2 Solar Angles

The following angles describe the daily motion of the sun:

Solar altitude angle, α : This is the sun's angular height above the horizon. Also referred to as the solar elevation, it ranges from 0 to 90° and is the complement of the solar zenith angle.

Solar zenith angle, θ_z : This is also called the zenith distance and is the angle between the local zenith and the line joining the observer and the sun. It is an angle between 0 and 90° .

Solar azimuth angle, ϕ : The solar azimuth is the angle at the local zenith, between the plane of the observer's meridian and the plane of a great circle passing through the zenith and the sun. It is measured east positive, west negative, (south zero) and hence varies between 0° and $\pm 180^\circ$.

Hour angle, α : The hour angle is measured at the celestial pole between the observer's meridian and the solar meridian. Starting from midday, it changes 15° per an hour. The relationship between the solar angles is given by the following equations:

$$\cos\theta_z = \sin\delta\sin\phi + \cos\delta\cos\phi\cos\omega = \sin\alpha,$$

$$\sin\phi = \frac{\cos\delta\sin\omega}{\cos\alpha},$$

where δ and ϕ are the declination and latitude angles, respectively. The declination angle was defined above and the latitude angle is defined as the angle between a line from the earth's center to a point on the earth and the equatorial plane [7,9].

3.3 Components of solar radiation

From the Earth, the solar disk subtends a solid angle of about 0.5° on average. Due to the eccentricity of the Earth's elliptical orbit, the distance from the Earth to the Sun varies throughout the year which results in a variation in the intensity of the solar radiation at the top of the atmosphere. The Sun thus acts as a quasi point source, illuminating the Earth with very nearly parallel rays of radiation, as shown in figure 3.4. This quasi-collimated beam is the extraterrestrial direct beam, or extraterrestrial radiation, referred to as ETR [6].

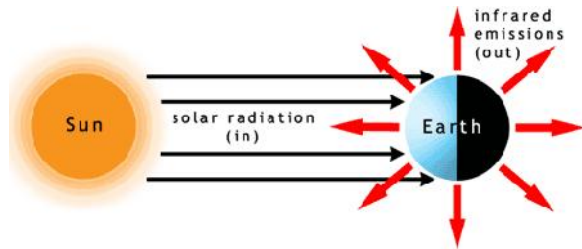


Figure 3.4: Sun rays incident on the Earth's surface [10].

As the ETR beam traverses the atmosphere, interaction between the photons in the beam and the atmosphere result in scattering and absorption of photons out of the beam into random paths in the atmosphere. Scattered photons (mostly at short wavelengths) produce the diffuse sky radiation, which we will denote by D . The remaining unabsorbed and unscattered photons, still nearly collimated, constitute the direct beam radiation, responsible for the casting of shadows, which will be denoted as B . The total radiation flux on a horizontal surface in the presence of diffuse and beam radiation is often called "total" or "global" radiation. We will denote this global solar radiation on a horizontal surface as G . The term "global" refers to the concept that the radiation on a horizontal surface is received from the entire 2π solid angle of the sky dome. The difference between G at ground level and its corresponding value at the top of the atmosphere is what has been absorbed or reflected away by the atmosphere. On average, the Earth reflects about 29% of the incident solar irradiance back to space (see figure 3.5) [6].

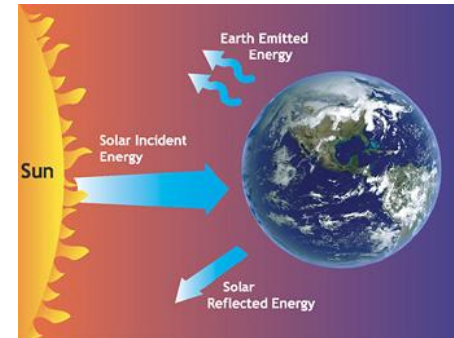


Figure 3.5: Incident, emitted and reflected solar energy [11].

The total solar radiation received by a tilted (non-horizontal) surface is a combination of direct beam, diffuse sky, and additional radiation reflected from the ground (which we will denote as R), and should be referred to as total hemispherical radiation on a tilted surface. However, it is most often described by the simpler term "global tilted" radiation. Figure 3.6 illustrates the various components of ground received solar radiation on intercepting surfaces.

The incidence angle (i) of the solar beam upon a horizontal surface is equal to the solar zenith angle (z), i.e., the complement of the solar elevation (h). Thus the basic relation between the total global horizontal radiation G , direct beam radiation B at normal incidence, and diffuse radiation D on a horizontal surface can be described by:

$$G = B\cos(z) + D \text{ [6].}$$

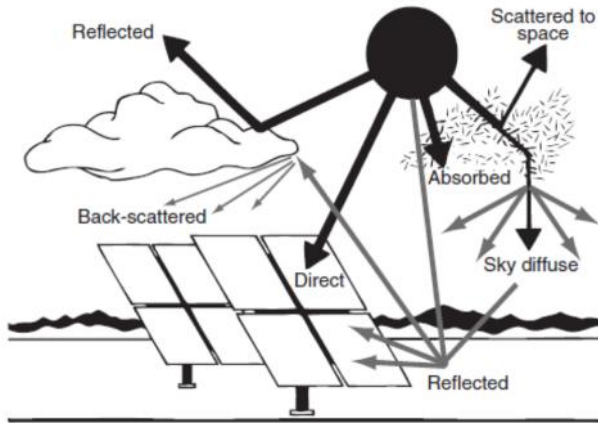


Figure 3.6: Solar radiation components segregated by the atmosphere and surface. Many interactions take place once the solar irradiance reaches the ground [6].

4.4 Solar radiometry instrumentation

The most common applications of broadband radiometry are the monitoring of incoming solar radiation to evaluate the solar resource available to various energy conversion technologies, and the monitoring of the performance of conversion systems once deployed. The sensing and recording of the solar resource during such endeavors involves selecting, calibrating, installing,

monitoring, and maintaining radiometric sensors of adequate accuracy and suitable configuration to meet the engineering needs of the test or measurement. There have been a large variety of instruments developed for solar radiation measurements. These can be broadly classified into 6 groups [6]:

- (1) Pyrheliometers: this class of instruments measure the direct (beam) solar irradiance with the receiving surface normal to the incident irradiation.
- (2) Pyranometers: these instruments measure the solar irradiance emanating from the total hemisphere within 180° field of view. They are used to measure both global irradiance and diffuse irradiance separately.
- (3) Sunphotometers: these are pyrheliometers which use narrow band interference filters for spectral measurements to obtain atmospheric characteristics such as aerosol and water vapour concentration.
- (4) Pyrgeometers: also referred to as long wave radiometers, they measure the atmospheric/terrestrial radiation on a horizontal surface at ambient temperature. Special filters can be added to measure specific components of the terrestrial radiation.
- (5) Pyrriadiometers: these measure the total radiation both in the solar and terrestrial wavelengths
- (6) Illuminometers: these measure the illumination energy – the light energy producing the effect of vision – in the visible spectrum [6].

Standardization of Radiation Measurements

Similar to other instruments, the characteristic properties of radiation measuring instruments are most likely to change with time. This is due to exposure to weather elements, handling of the instruments and various other factors that may affect the accuracy and precision of measurements. Therefore, in order to maintain a high degree of accuracy, it is important that the instruments are periodically calibrated against a reference standard instrument and their accuracy re-established at regular intervals [6].

The solar radiation community has developed an international solar radiometric scale through the World Meteorological Organization, Commission for Instrumentation and Methods of Observation (CI-MO). The current solar radiometric reference scale is called the World Radiometric Reference, or WRR. The WRR was established in 1977 through special intercomparisons of 15 absolute (electrical substitution calibrated) cavity pyrheliometers of 9 different designs. (WMO, 1983) [12].

The World Radiation Center at Davos, Switzerland is responsible for the maintenance of the radiation standard instruments constituting the WSG which is used to define the WRR. To monitor the performance and ensure long term stability of the WRR, the instruments of the WSG are inter-compared at least once a year [6].

Factors affecting accuracy of the radiation measurements [6]:

Resolution: this is the smallest change in the parameter that the instrument is capable of measuring with certainty.

Long-term stability: the drift in calibration should not be more than $\pm 2\%$ per year.

Change in sensitivity/response due to variations in ambient temperature: the thermopile instruments show a change in response when there is a change in instrument temperature.

Non-linearity of response: the instrument response should be linear to within $\pm 2\%$ over the range of irradiances normally received.

Variation in spectral response: this is due to change in blackness of the receiving surface and transmission effect of aperture windows, and should be less than $\pm 2\%$.

Cosine and azimuthal error: the sensor response varies with solar elevation giving rise to Lambert's cosine error. The response is proportional to the cosine of the zenith angle of the beam.

Radiative cooling (at night): this gives rise to zero suppression.

Instrument leveling: very important in terms of obtaining accurate measurements [6].

Direct/Beam radiation measurements by a Ppyrheliometer:

Direct/ beam radiation is measured by an instrument called a Ppyrheliometer. The sensor surface of the ppyrheliometer, which is a quartz window, is always normal to the incident radiation. The window material of the ppyrheliometer defines the spectral measurement range of the instrument. In general about 97 – 98 % of the solar radiation spectrum will be transmitted through the window and will be absorbed by the detector [13].

The detector is a thermopile sensing element is made up of a large number of thermocouple junction pairs connected electrically in series. The absorption of thermal radiation by one of the thermocouple junctions, called the active (or 'hot') junction, increases its temperature. The differential temperature between the active junction and a reference ('cold') junction kept at a fixed temperature produces an electromotive force directly proportional to the differential temperature created. This is a thermoelectric effect. The sensitivity of a ppyrheliometer depends on the individual physical properties of the thermopile and construction. The sensitivity of each thermopile is unique and therefore each radiometer has unique calibration factor, even with the

same radiometer model. On the top surface of the sensor a black paint is deposited which has a very rough structure containing many micro-cavities that effectively ‘‘trap’’ more than 97 % of the incident radiation in a broad spectral range. The black painted sensing element forms the detector. Considering the long-term stability of the instrument, the black paint is one of the most crucial and delicate parts of the pyrheliometer [4]. Figure 3.7 (a) and (b) is a Normal Incidence Pyrheliometer (NIP).

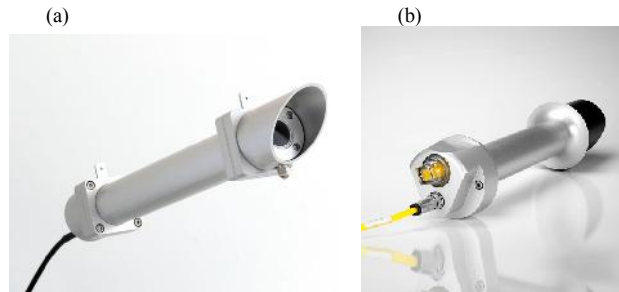


Figure 3.7: Normal Incidence Pyrheliometer (a) front and (b) rear view [14,15].

Global and Diffuse radiation measurements by a Pyranometer:

Global radiation is measured by a pyranometer whose sensing element is a blackened thermopile sensor. Figure 3.8 is a typical pyranometer and figure 3.9 illustrates the working principle.

Radiant energy strikes the pyranometer and is absorbed the the blackened sensor. The heat generated flows through a thermal resistance to the heat sink, which is the body of the pyranometer. The difference in temperature across the thermal resistance of the disk is converted into a voltage. The sensor is shielded by a double dome structure to prevent heat loss due to wind and rain, and thermal radiation loss due to the environment.

Diffuse (scattered) is measured using a pyranometer with an additional component, usually a shading ball/ring/disk. The shading device casts a shadow on the pyranometer sensor therefore shielding the sensor from the direct irradiance. This shadow remains on the sensor from sunrise

to sunset throughout the year. By screening the direct radiation component the diffuse component can be measured. The diffuse radiation is caused by multiple scattering through various atmospheric constituents, scattering due to clouds, as well as reflection from the ground. Pyranometer with the shading device is shown in figure 4.10.



Figure 3.8: Ushaded pyranometer [16].

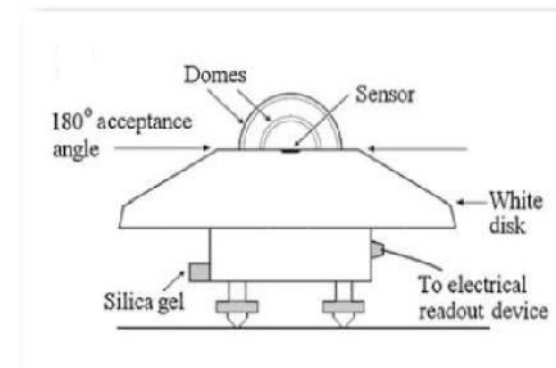


Figure 3.9: Illustration of the working principle of a pyranometer [17].



Figure 3.10: Pyranometer with shading ring device for diffuse measurements [18].



Figure 3.11: Pyranometer with shading ball device for diffuse measurements [19].

3.5 Solar Radiometry Station

The monitoring of ground received solar radiation plays an important role in the implementation of solar powered technologies. Adequate knowledge of the solar resource will allow efficient and cost-effective design of solar powered devices.

Solar resource monitoring is vital for both small and large scale solar systems. For example, solar water heaters installed on residential rooftops need to be properly sized for optimal use. On the otherhand, large grid-connected photovoltaic plants require knowledge of the solar irradiance in order to estimate electricity generation capacity.

A typical solar radiometry station consists of the instruments mentioned above. Generally, there is one pyrheliometer and two pyranometers (one for global and the other for diffuse measurements) mounted on a sun tracker. The system is sometimes connected to a photovoltaic panel to avoid any disruption in measurements due to power outages. There is usually a high cost involved in setting up a solar radiometry station and as a result the pyranometer measuring diffuse irradiance is omitted and these values are derived theoretically.

In addition to setting up of the station, it also requires personnel to regularly clean the instruments and carry out regular maintenance.

Some examples of existing solar radiometry networks is given in the table below [20].

Table 4.1: Existing solar radiometry networks [20].

Data Source	Website
Baseline Surface Radiation Network (BSRN)	www.gewex.org/bsm.html
World Radiation Data Centre (WRDC)	wrdc.mgo.nrel.gov
Surface Radiation Network (SURFRAD)	www.esrl.noaa.gov/gmd/grad/surfrad/
Atmospheric Radiation Measurement (ARM)	www.arm.gov
University of Oregon Solar Radiation Monitoring Laboratory (SRML)	solardat.uoregon.edu/index.html
Australian Bureau of Meteorology (BOM)	www.bom.gov.au/climate/data-services/solar/
South African Universities Radiometric Network (SAURAN)	www.sauran.net

References:

- [1] Grum F., Becherer R.J., (1979), "Optical Radiation Measurements: Radiometry" Volume I.
- [2] Palmer J.M., Grant B.G., (2009), "The Art of Radiometry".
- [3] www.science3d.org/content/basic-principles-x-ray-tomography-x-rays.
- [4] Srivastava G.P., (2008), 'Surface Meteorological Instruments and Measurement Practices'.
- [5] Wolfe W.L., (1998), "Introduction to Radiometry".
- [6] Badescu V., (2008), "Modelling Solar Radiation at the Earth's Surface".
- [7] Govender P., "Construction and Analysis of the Receiver for a Solar Thermal Cooker System", (2013), MSc Thesis.
- [8] <http://www.physicalgeography.net>.
- [9] Twidell J., Weir T., (2006). "Renewable Energy Resources".
- [10] <http://www.helpsavetheclimate.com/climatetheory.html>.
- [11] http://www.esrl.noaa.gov/gmd/outreach/faq_cat-1.html.
- [12] Myers D., "Radiometric Instrumentation and Measurements Guide for Photovoltaic Performance Testing", National Renewable Energy Laboratory, 1997.
- [13] Kipp and Zonen, CHP 1 Instruction Manual.
- [14] <https://en.wikipedia.org/wiki/Pyrheliometer>.
- [15] <http://www.azocleantech.com/equipment-details.aspx?EquipID=72>.
- [16] <http://www.kippzonen.fr/>.
- [17] http://www.globalspec.com/learnmore/sensors_transducers_detectors/weather_sensing/solar_radiation_instruments.
- [18] <http://www.kippzonen.com/Product/42/CM-121B-C-Shadow-Ring#.Vbs8kLOqpBc>.
- [19] http://www.volker-quaschnig.de/articles/fundamentals1/index_e.php.
- [20] Brooks M.J., du Clou S., van Niekerk W.L., Gauche' P., Leonard C., Mouzouris M.J., Meyer R., van der Westhuizen N., van Dyk E.E., Vorster F.J., "SAURAN: A new resource for solar radiometric data in Southern Africa", Journal of Energy in Southern Africa, Volume 26 (1), 2015.